


Oxide cathodes for sodium-ion batteries: Designs, challenges, and perspectives

Tao Chen^{1,2} | Baixue Ouyang^{1,2} | Xiaowen Fan^{1,2} | Weili Zhou¹ | Weifang Liu^{1,3} | Kaiyu Liu^{1,2} 

¹College of Chemistry and Chemical Engineering, Central South University, Changsha, P.R. China

²Hunan Provincial Key Laboratory of Chemical Power Sources, College of Chemistry and Chemical Engineering, Central South University, Changsha, P.R. China

³College of Chemistry and Chemical Engineering, Hunan University, Changsha, P.R. China

Correspondence

Weifang Liu, College of Chemistry and Chemical Engineering, Hunan University, Changsha 410082, P.R. China.
Email: 380646837@qq.com

Funding information

National Natural Science Foundation of China, Grant/Award Number: 21471162; Hunan Provincial Innovation Foundation for Post graduate, Grant/Award Number: 502211822

Abstract

Sodium-ion batteries (SIBs), which are an alternative to lithium-ion batteries (LIBs), have attracted increasing attention due to their low cost of Na resources and similar Na storage mechanism to LIBs. Compared with anode materials and electrolytes, the development of cathode materials lags behind. Therefore, the key to improving the specific energy and promoting the application of SIBs is to develop high-performance sodium intercalation cathode materials. Transition-metal oxides are one of the most promising cathode materials for SIBs owing to their excellent energy density, high specific discharge capacity, and environmentally friendly nature. In the present work, the latest progress in the research of transition-metal oxides is summarized. Moreover, the existing challenges are discussed, and a series of strategies are proposed to overcome these drawbacks. This review aims at providing guidance for the development of metal oxides in the next stage.

KEYWORDS

cathodes, layered oxides, oxygen reduction, phase transition

1 | INTRODUCTION

As energy consumption and demand continue to increase, there is a growing need for low-cost, efficient, long-life, and secure renewable energy storage systems. Renewable energy, including solar energy, wind energy, tidal energy, water energy, geothermal energy, marine energy, and biomass energy, and so forth,¹ has a natural self-renewable function. Integrating these regional and intermittent sources of energy into low-cost and efficient large-scale

electrical energy storage systems is the key to solving the energy crisis. Rechargeable batteries represent one of the most popular electrical energy storage systems due to their high conversion efficiency and eco-friendly feature.^{1–3} As a kind of rechargeable batteries, lithium-ion batteries (LIBs) have been widely used in mobile phones, laptops, digital cameras, electric tools, and other fields because of their outstanding advantages such as high energy density, high working voltage, long cycle life, low self-discharge rate, and environmentally friendly nature, and their applications are

Tao Chen and Baixue Ouyang are joint first author and contributed equally to this study.

This is an open access article under the terms of the Creative Commons Attribution License, which permits use, distribution and reproduction in any medium, provided the original work is properly cited.

© 2022 The Authors. *Carbon Energy* published by Wenzhou University and John Wiley & Sons Australia, Ltd.

gradually expanding to new energy vehicles and other energy storage fields.^{4,5}

However, the growing market of LIBs is inevitably leading to shortage of lithium resources and increase in the price of lithium. Therefore, it is necessary to develop a new energy storage system with abundant resources and low price to replace LIBs. Due to its rich natural resources, low price, environmentally friendly nature, and similar electrochemical properties to LIBs, the sodium-ion battery (SIB) system has attracted considerable attention in recent years, providing a new choice for electrical energy storage.^{6–9} Sodium is the sixth most abundant element in the crust (2.75%), and the cost of raw material of Na_2CO_3 is approximately 25 times lower than that of Li_2CO_3 .^{10–12} Besides, sodium does not alloy with aluminum, so aluminum, which is cheaper than copper, is widely used as a negative collector fluid (the anode collector of LIBs is copper). Therefore, SIBs are expected to be the alternative to LIBs. During the charge process, Na^+ is extracted from the cathode and then inserted into the anode through the electrolyte, while the electrons flow into the anode through the external circuit to maintain the charge balance. The discharge process is just the opposite. Nevertheless, it is difficult for SIBs to exceed LIBs in terms of energy density because of the larger weight of sodium and lower standard electrochemical potential than that of lithium.^{13,14} In addition, SIBs show slower diffusion kinetics than LIBs due to the larger ionic radius of Na^+ (1.02 Å) than that of Li^+ (0.76 Å), which poses a challenge to the exploration of excellent electrode materials for SIBs. Under this circumstance, SIBs are suitable for applications where cost-effectiveness rather than energy density is the most critical issue, such as large-scale electrical energy storage systems.¹⁴ As a result, SIBs have once again generated attention in terms of research as low-cost rechargeable batteries.¹⁵

Among all the international studies in the field of SIBs, the development of cathode materials lags behind that of anodes and electrolytes, which thus makes the cathode the key component to determine the energy density and cost of the SIB system.^{16,17} To develop suitable cathode materials with high redox potential, high reversible capacity, excellent Na diffusion ability, and good cycling stability, several groups of materials have been investigated in the past few years, including metal oxides,^{18,19} polyanionic compounds,²⁰ hexacyanoferrates,²¹ and organic compounds.²²

Prussian blue compounds are a kind of promising cathode materials that possess high operating voltage and reversible capacity, whereas defects are easily formed in this material, leading to a decrease in the overall capacity and cycling stability.²³ The stable structures of polyanionic compounds ensure their higher circulability and safety; moreover, simple modification of ion substitution or

doping is also a characteristic of these materials.²⁴ However, the relatively low conductivity and volumetric energy density limit their development. Organic compounds are a new type of energy storage material with wide application prospects.²² The significant advantages of these materials, such as high theoretical specific capacity, abundant raw materials, environmental friendliness, low price, and flexible structure design, have attracted a lot of cutting-edge expectations. Future research of organic materials will focus on the construction of suitable structures and enhancements of the working voltage and cycle stability. In addition, some amorphous oxides also show excellent sodium ion storage capacity through certain interesting surface reactions, whereas the specific reaction mechanism of these reactions is not clear so far. Among them, transition-metal oxides (Na_xTMO_2 , in which TM represents transition-metal elements) are considered as one of the most promising cathodes due to their superior energy density, high reversible capacity, high operating potential, and ease of synthesis.^{25–28} In addition, the electrochemical properties of different transition-metal oxides are quite different, so two or more different metals can be mixed to form Na_xTMO_2 to obtain cathodes with good performance. Interestingly, some oxides made of partial metal elements, such as iron (Fe) and Cr, show good electrochemical properties in SIBs, but they are inert in LIBs.^{29,30}

In this review, recent progress in research on advanced Na_xTMO_2 cathode materials is summarized. Several challenges are also summed up, including irreversible phase transition, insufficient specific reversible capacity, instability of material surface, and high cost of Co/Ni-layered oxides. Besides, the mechanism of phase transition during the charge and discharge process is also introduced to reveal the relationship between the structure and performance in depth. Furthermore, a series of strategies to overcome these issues and some new perspectives are discussed, which provide theoretical guidance for the design of superior cathode materials. Future work should focus on the strategies to suppress irreversible phase transition, improve air stability, enhance overall performance, and further reduce the cost.

2 | OVERVIEW OF TRANSITION-METAL OXIDE CATHODES

2.1 | Structural classification

As early as the 1980s, oxide materials for SIBs have been studied by Hagenmuller et al. and are considered to be a good substitute for LIBs due to the low cost of Na resources and high energy density. At present, tunnel-type oxides and layered oxides are the two main types of

Na_xTMO_2 cathodes. Layered materials can be divided into two main categories: P2 and O3 types according to the coordination environment of Na^+ and the number of stacking sequences of oxygen layers.³¹ “P” and “O” represent the coordination environment of Na^+ , and the following number represents the quantity of repeated oxygen layers within the unit cell. The oxygen stacking sequence of P2-type Na_xTMO_2 corresponds to AB BA, and all Na^+ is embedded in the trigonal sites (Figure 1A). Furthermore, Na^+ is located at two different trigonal sites: Na_e and Na_f . Na_e is adjacent to six MO_6 octahedrons, whereas Na_f is adjacent to two MO_6 octahedrons. Meanwhile, P2-type Na_xTMO_2 belongs to a hexagonal system with a space group of $P63/mmc$. In the P2 phase, Na ions occupy prismatic sites stably. When a certain amount of Na ions are deintercalated, MO_6 octahedral layers begin to slide to form an O2 phase (Figure 1B) or a P'2 phase in which the prime symbol (') is used to represent the deformation of a hexagonal lattice.³² The O2 phase with a decreased layer spacing is not conducive to the deintercalation/intercalation of Na, leading to poor cycle stability. In O3-type Na_xTMO_2 , all Na^+ is located at octahedral sites, which correspond to an $R\bar{3}m$ space group with an oxygen stacking sequence of AB CA BC (Figure 1C).¹⁴ Furthermore, with the deintercalation of Na^+ in O3-type Na_xTMO_2 , Na^+ ions on prismatic sites tend to move to more stable sites to become energetically stable; meanwhile, vacancies are formed. Through the slip of transition-metal oxide sheets, new prismatic sites are subsequently generated. As a result, the stacking sequence of oxygen is converted into AB BC CA, forming the P3 phase (Figure 1D). Tunnel-type oxides belong to an orthorhombic crystal system with the $Pbam$ space group,³³ and they mainly consist of an MO_5 pyramid and an MO_6 octahedron to form S-shaped and pentagonal tunnels in which Na^+ is located at three different sites (Figure 1E). This unique open structures and interconnected large tunnels permit multiple reversible phase transitions during the Na^+ deintercalated/intercalated process.

2.2 | Anion reduction reaction

Oxygen redox is an emerging topic to enhance the practical capacity in the application of both LIBs and SIBs. In the early 2000s, the layered material $\text{Li}[\text{Li}_{1/3}\text{Mn}_{2/3}]\text{O}_2$ delivered a capacity of 300 mAh g^{-1} beyond the theoretical limit, attributed to the transition-metal redox.³⁴ The frontier characterization later proved that the additional capacity contribution is associated with oxygen loss from the oxide lattice.³⁵ Subsequently, the application of anions in SIBs to increase the capacity of the battery has also been widely studied.^{36,37} The mechanism and structural

evolution of anion reduction are still at the exploratory stage. In general, the formation of nonbonding oxygen 2p states is considered to be closely related to the reduction of oxygen.^{38,39} It is found that when some of the non-TMs with full *d* shell elements, such as Li, Na, Mg, Zn, or vacancies, replace the transition-metal sites in the layered metal oxides, the formation of a peroxo-like O–O bond can be facilitated due to a weaker metal–oxygen bond.⁴⁰ First of all, doping of these ions leads to a decrease in the covalent bond strength of M–O and gradually shifts the oxygen 2p nonbonding band up near the Fermi level, triggering an extra redox process. In addition, as shown in Figure 2A, the inserted elements in the TM layers are sectionally removed from the lattice, therefore leaving plenty of vacancies in the host lattice. The formation of nonbonding oxygen 2p orbitals and the generation of a “Na–O–vacancy” or even a “vacancy–O–vacancy”

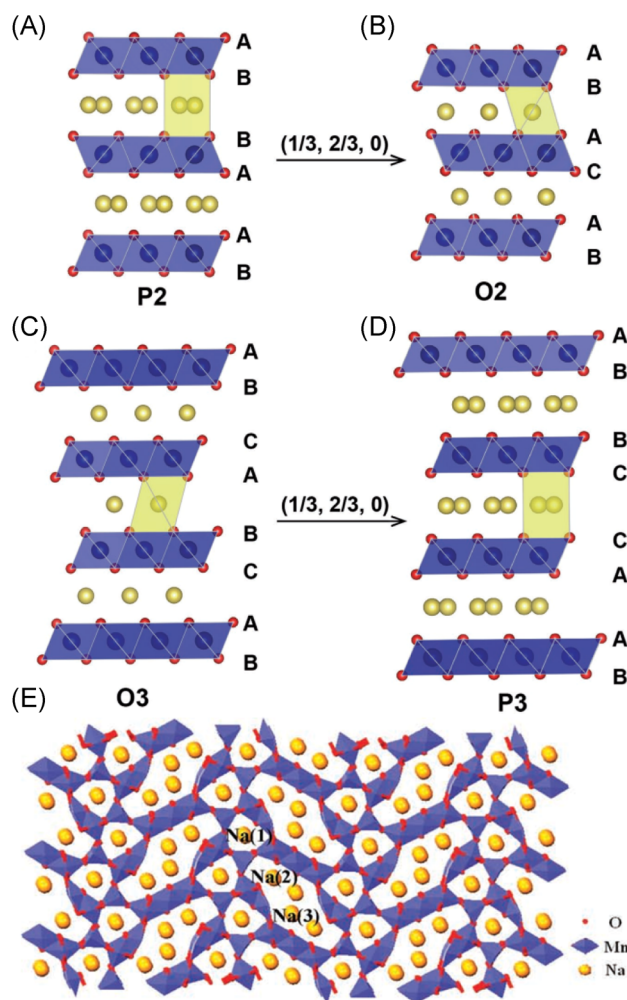


FIGURE 1 Schematic crystal structure of Na_xTMO_2 for (A) P2 type, (B) O2 type, (C) O3 type, and (D) P3 type. Reproduced with permission: Copyright 2017, Wiley.¹⁴ (E) Tunnel type. Reproduced with permission: Copyright 2011, Wiley³³

configuration (as shown in Figure 2B) ultimately trigger the O-redox reaction.^{41–43} On the one hand, oxygen redox reactions can break through the theoretical capacity to yield a higher energy density. On the other hand, the loss of lattice oxygen and migration of TM ions may cause undesirable phase transition and irreversible structural changes, thereby reducing the cyclic properties. Hence, designing reversible oxygen reduction at high voltage and suppressing irreversible phase transition during the charge–discharge process are the focus of the following research.

3 | CHALLENGES AND STRATEGIES

Although results of numerous studies show that transition-metal oxides are a category of promising cathode for SIBs, some major drawbacks hinder their development.

Most of the layered transition-metal oxides in P2 and O3 phases undergo a series of irreversible phase transitions during the extraction of Na⁺ due to the slip of oxygen layers. When a certain amount of Na⁺ ions are extracted from P2 phase oxides, some MO₆ octahedra sheets begin to glide to form octahedral sites, resulting in transformation into the O2 phase with a unique AB AC AB oxygen stacking.⁴⁴ The irreversible P2–O2 phase transition leads to rapid structural collapse, which accelerates the capacity decay. Compared with P2-type structures, most O3 structural materials undergo more complex phase transformation. For example, the O3 → (O3 + O'3) → P3 → P'3 → (P'3 + P3'') → P3''

complex phase transition is observed during the extraction of Na⁺.⁴⁵ When Na is extracted about 25% from the O3 phase, the formation of vacancies induces Na⁺ to shift from the octahedral site to the trigonal site to maintain the most stable state. As a result, the oxygen layers begin to glide and the stacking order of the oxygen layers changes from “AB CA BC” to “AB BC CA,” which occurs in all the O3-type compounds.⁴⁶ Phase transition alters the diffusion mechanism of sodium ions in the plane.⁴⁷ There are two strategies that can be used to resolve this issue. Since most of the phase transitions occur in the high-voltage range, the first strategy is to limit the high cut-off voltage to suppress the phase transitions.⁴⁸ However, this method may lead to low average operating voltage and insufficient capacity in the system. After the P2–O2 phase transition is eliminated by limiting the high cut-off voltage to 4.1 V, Na_xMn_{2/3}Ni_{1/3}O₂ shows a 95% capacity retention rate rather than previous 65% retention.⁴⁷ Another strategy is to substitute transition metals with some electrochemical inactive metal elements to stabilize the structure and delay structural transitions, such as Li, Mg, Al, Zn, and so forth.^{49–52} Meanwhile, doping some of the active metals also shows suppression to phase transition, such as Cu and Fe.^{53,54} Various layered oxides containing Fe or Cu show high operating voltages through redox reactions of Fe³⁺/Fe⁴⁺ or Cu²⁺/Cu³⁺ at high voltages, respectively. Their multielectron transfer process guarantees ideal discharge-specific capacity, so they show high structural stability in the high-voltage range.

To ensure a high operating voltage and improve the conductivity of the system, Ni and Co become indispensable

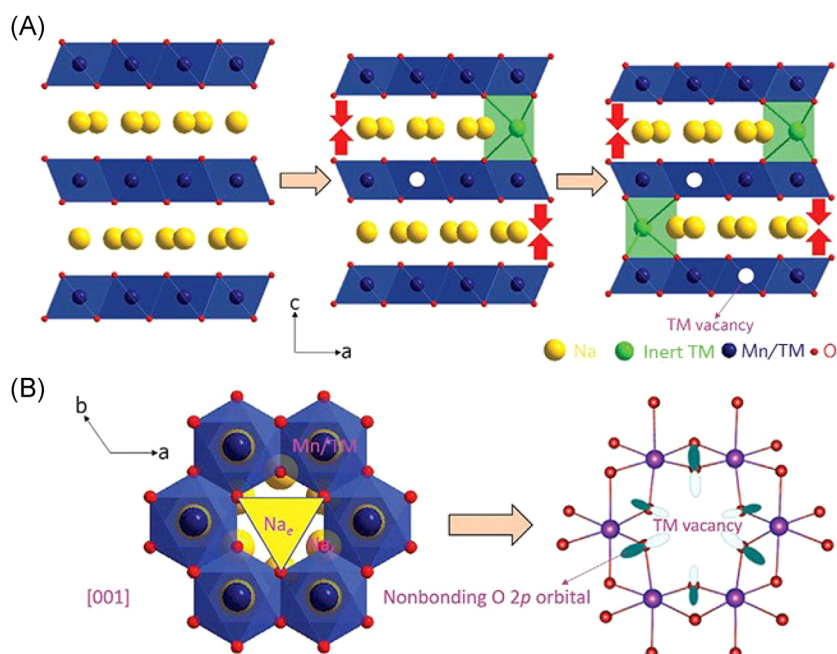


FIGURE 2 (A) Crystallographic evolution of Na_xTMO₂ with inserted element substitution and (B) local coordination environment of Na⁺ and the vacancy above Na_e in the TM layer. Reproduced with permission: Copyright 2020, Wiley⁴¹

elements to help achieve superior performance. However, Ni and Co are widely used in LIBs as $\text{LiCo}_{1-x-y}\text{Ni}_x\text{Mn}_y\text{O}_2$ cathodes. With the expansion of the electric vehicle market, the costs of Ni and Co have increased rapidly. Therefore, it is essential to strike a balance between performance and the cost of the final application. Development of Ni/Co-free layered oxides with superior performance can be an effective strategy to solve this issue. Air-stable and Co/Ni-free layered O3- $\text{Na}_{0.9}[\text{Cu}_{0.22}\text{Fe}_{0.30}\text{Mn}_{0.48}]\text{O}_2$ has been reported as an advanced cathode material for SIBs.⁵⁵ This cathode can store a reversible discharge-specific capacity of $\approx 100 \text{ mAh g}^{-1}$ with 3.2 V average storage voltage. The full cell coupled with a hard carbon anode shows an excellent energy density of 210 Wh kg^{-1} with 90% round-trip energy efficiency, indicating the high industrial feasibility of this system. The full cell also offers 74% of the initial capacity at a current density of up to 6 C.

For a layered oxide Na_xMO_2 cathode, the limited number of Na ions leads to insufficient specific capacity. The theoretical capacity of P2-type Na_xMO_2 is about 170 mAh g^{-1} , while that of O3 is about 240 mAh g^{-1} . In the practical charging and discharging process, due to the presence of polarization, it is hard to achieve the value of theoretical capacity, and even most layered oxides show a capacity of no more than 150 mAh g^{-1} . One of the effective strategies is to construct sodium-excess metal oxides Na_2MO_3 .^{56–58} Ordered Na_2RuO_3 with honeycomb-ordered $[\text{Na}_{1/3}\text{Ru}_{2/3}]\text{O}_2$ slabs offers a superior reversible specific capacity of 180 mAh g^{-1} .³⁷ Furthermore, inducing the generation of anionic redox reaction is also an effective strategy to increase the storage capacity of layered oxides.^{59–63} The substitution of inactive elements (Li, Mg, Al, etc.) is usually used to trigger the lattice oxygen redox reaction of oxygen, especially Li substitution. For instance, Chen et al. reported a P2-type $\text{Na}_{0.72}[\text{Li}_{0.24}\text{Mn}_{0.76}]\text{O}_2$, showing an exceptionally high reversible capacity of about 270 mAh g^{-1} and energy density of 700 Wh kg^{-1} between 1.5 and 4.5 V.⁶⁴ To date, it offers the highest specific discharge capacity among all the cathodes of SIBs. It is confirmed that reversible oxygen reduction provides additional capacity beyond the theoretical value. In addition, the P2 structure can still be maintained even after the complete removal of Na^+ ions with minimal volume change (1.35%), which is caused by the decrease in Coulombic repulsion associated with an anionic redox reaction.

Furthermore, layered oxides are sensitive to the surrounding environment and prone to absorbing water and CO_2 molecules into the alkali metal layers to form Na_2CO_3 and NaOH on the surface when exposed to air.⁶⁵ The oxidation reaction between layer oxides and water or H^+/Na^+ exchange results in the extraction of Na ions and subsequent structural variation, which therefore leads to the deterioration of electrochemical performance and increases the cost

of material preservation and transportation.⁶⁶ Therefore, it is indispensable to develop air-stable layered oxide cathode materials.⁶⁷ On the other hand, it can also be effectively solved by designing a multifunctional protective layer that could limit the undesirable side reactions with air.⁶⁸

4 | TRANSITION-METAL OXIDES

4.1 | Single-metal oxides

It has been proven that a series of single transition-metal (Mn, Co, Ni, Fe, V, Cr, etc.) oxides show electrochemical activity as Na-host materials for SIBs. In general, current research has gradually shifted from single-metal oxides to ternary or multiple oxides. However, the study of single-metal oxides, which is conducive to understanding the properties of each element and laying the foundation for the synthesis of multimetal oxides with comprehensive properties, is still vital.

Na_xMnO_2 oxides are attractive due to the cost-effectiveness of manganese.^{69,70} Na_xMnO_2 shows a 3D tunnel structure when x is less than 0.44, and it presents a layered structure at higher Na content ($x > 0.5$). In early 1985, O'3-type $\alpha\text{-NaMnO}_2$ with a $C2/m$ space group was first investigated by Mendiboure et al.⁷¹ It was shown that $\alpha\text{-NaMnO}_2$ has poor reversibility of Na extraction/insertion. In addition, $\alpha\text{-NaMnO}_2$ delivers an initial discharge capacity of 185 mAh g^{-1} between 2.0 and 3.8 V at 0.1 C, corresponding to 0.85 Na deintercalation (Figure 3A).⁷² $\beta\text{-NaMnO}_2$, which is composed of zigzag layers of edge-sharing MnO_6 octahedra, also presents a high capacity of 190 mAh g^{-1} at a rate of 0.05 C, showing a space group of $Pmnm$.⁷³ The structure is prone to collapse at low sodium content. At the same high sodium content, low temperatures contribute to the synthesis of $\alpha\text{-NaMnO}_2$ and high temperatures are beneficial for $\beta\text{-NaMnO}_2$. Besides, layered P2- Na_xMnO_2 delivers a capacity of more than 140 mAh g^{-1} at a current density of 0.1 mA cm^2 (Figure 3B). The continuous strains and distortions lead to gradual collapse of the structure during the insertion and extraction of Na^+ ions, resulting in a progressive reduction of capacity. The Jahn–Teller distortion caused by the asymmetric electron cloud of Mn^{3+} makes it difficult for Mn-based Na_xMnO_2 to maintain high structural stability.⁷² Komaba et al. prepared distorted P'2- $\text{Na}_{2/3}\text{MnO}_2$ via a single-phase synthesis route and investigated how the structure influences electrochemical reactions.⁷⁴ The distorted P'2 $\text{Na}_{2/3}\text{MnO}_2$ presents 216 mAh g^{-1} discharge capacity, corresponding to 590 Wh kg^{-1} . The P'2 phase is maintained during $0.25 < x < 0.80$ in Na_xMnO_2 , while it transforms into the OP4 phase during $x < 0.3$, as shown in Figure 3C.

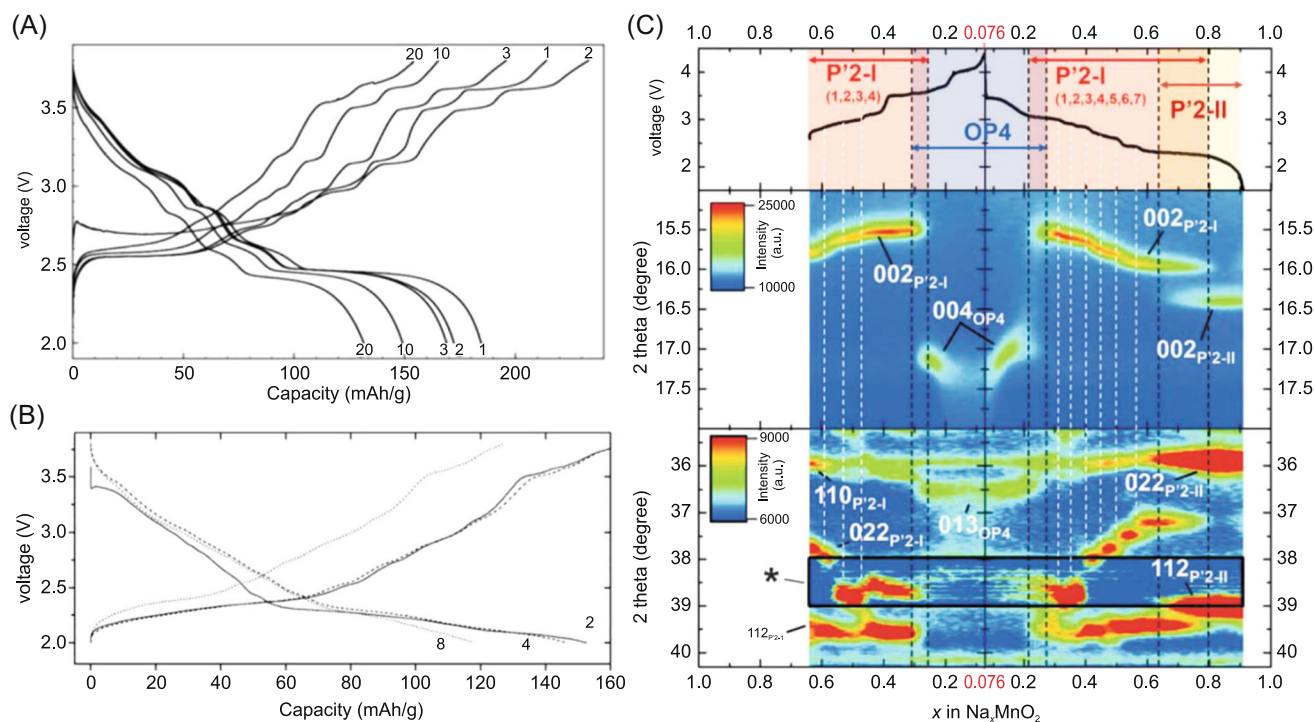


FIGURE 3 (A) Voltage profile of α -NaMnO₂ at 0.1 C. Reproduced with permission: Copyright 2011, The Electrochemical Society.⁷² (B) Charge-discharge curves of P2-Na_{0.6}MnO₂ in the voltage range of 2.0–3.8 V. Reproduced with permission: Copyright 2002, The Royal Society of Chemistry.⁷³ (C) Operando X-ray diffraction patterns of P'2-Na_{2/3}MnO₂ during the initial charge-discharge curves. Reproduced with permission: Copyright 2016, Wiley⁷⁴

Orthorhombic Na_{0.44}MnO₂ is a typical tunnel-type sodium storage material with the *Pbam* space group, which consists of interconnected and large tunnels. Li et al. have synthesized a tunnel Na_{0.44}MnO₂ nanoplate using a template-assisted sol-gel method.⁷⁵ It presents a discharge capacity of about 110 mAh g⁻¹ at 0.5 C with 97.8% retention after 100 cycles. Besides, Na₄Mn₉O₁₈ prepared using a polymer-pyrolysis method shows high crystallinity and a homogeneous nanowire structure, which provides a short diffusion path for Na-ion extraction and intercalation.³³ It also shows a superior capacity retention capability of 77% even after 1000 cycles at 0.5 C. To better regulate the structure of Na_{0.44}MnO₂, a series of synthesis strategies were attempted, including electrospinning,⁷⁶ hydrothermal synthesis methods,⁷⁷ ultrasonic sonochemical synthesis,⁷⁸ urea-based solution combustion,⁷⁹ and so forth.

As early as the 1980s, Na_xCoO₂ has been investigated for its similarity to LiCoO₂.⁸⁰ The electrochemical investigation of the P2-Na_xCoO₂ was conducted by Berthelot et al.⁸¹ In this study, based on in situ X-ray diffraction (XRD) analysis and the galvanostatic intermittent titration technique (GITT) electrochemical discharge curve for $x \geq 0.50$, the continuity of single-phase or two-phase domains is accurately identified during the sodium intercalation and extraction process. The peculiar Na⁺/vacancy

ordering results in nine single-phase domains in the range of $1 > x \geq 0.50$. Besides, research shows that the oxygen nonstoichiometric in Na_{0.7}CoO_{2-y} results in the formation of electron holes and an unstable tetravalent Co⁴⁺, which reduces conductivity, allowing more Na⁺ insertion to stabilize the charge balance.^{82,83} On the other hand, reversible structural transitions (O3 \leftrightarrow O'3 \leftrightarrow P') were found during the electrochemical process in O3-type Na_xCoO₂.⁸⁰ As shown in Figure 4A,B, Ceder's group revealed that O3, O'3, and P'3 phases were formed when the contents of x were 1.00, 0.83, and 0.67, respectively.⁸⁴ Moreover, the P2 phase was found in the range of $0.76 \geq x \geq 0.68$.

α -NaFeO₂ with the *R3m* space group was demonstrated to be a promising O3-type layered oxide for SIBs.⁸⁵ α -NaFeO₂ delivers a reversible capacity of 85 mAh g⁻¹ with a flat voltage plateau at 3.3 V.⁸⁶ The Fe³⁺/Fe⁴⁺ redox reaction contributes the main capacity in the charge and discharge process. The results of X-ray absorption spectroscopy (XAS) and XRD show that the reversible capacity and polarization decrease on charging above 3.5 V.^{87,88} The irreversible Fe migration from the Fe layer to the Na layer was confirmed by Li et al.⁸⁹ To suppress cation migration and reduce particle cracks, Ru-doped NaFeO₂ was prepared by Zhou and his group.⁹⁰ The well-ordered layered structure of Ru-doped NaFeO₂ restrains the distortion of Fe-O and thus inhibits the migration of Fe. As a result, it provides a

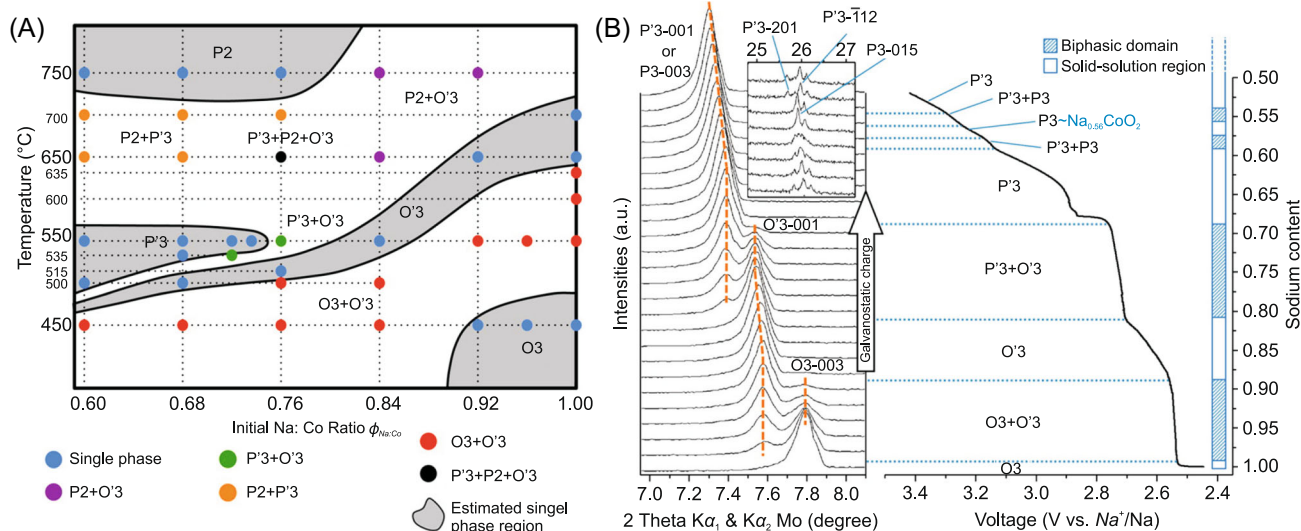


FIGURE 4 (A) Synthesis phase diagram of Na_xCoO_2 as a function of the precursor Na:Co ratio $\phi_{Na:Co}$ (X axis) and the sintering temperature (Y axis); (B) electrochemistry and in situ X-ray diffraction (XRD) spectra of $O3-Na_xCoO_2$. The galvanostatic electrochemical charge curve (right side) and simultaneous in situ XRD scans (left side) are shown. Reproduced with permission: Copyright 2014, American Chemical Society⁸¹

reversible capacity of 120 mAh g^{-1} with 80% retention after 100 cycles. In situ XAS results show no significant shift to high energy in the Fe K-edge, demonstrating that the charge compensation is not through the Fe^{3+}/Fe^{4+} redox reaction when Na^+ ions are extracted from the $NaFeO_2$.⁹¹ These results suggest that oxygen redox activity supports the charge compensation. When more than 0.5 Na is extracted from $O3-NaFeO_2$, a Fe_3O_4 product is formed, which leads to the irreversibility of $NaFeO_2$. Besides, Saurel et al. combined the potential intermittent titration technique, in situ XRD, and electrochemical impedance spectroscopy to track Fe migration and studied its effect on Na diffusion.⁹² It is confirmed that the migration of Fe shows an adverse effect on the capacity and dynamic properties.

Moreover, layered Na_xNiO_2 is also attractive due to its high potential platform of Ni^{2+}/Ni^{3+} and Ni^{3+}/Ni^{4+} .⁹³ Monoclinic $O'3$ -type $NaNiO_2$ delivers a 120 mAh g^{-1} reversible capacity between 1.25 and 3.75 V.⁹⁴ In the process of Na extraction, Na_xNiO_2 undergoes complex phase transitions from $O'3$, $P'3$, $P''3$, $O''3$, to $O'''3$ phase in sequence as illustrated in Figure 5.^{95,96} The capacity loss of the first cycle is obvious with only 89% Coulombic efficiency, and the Coulombic efficiency reaches 98% from 2 to 25 cycles. The irreversible phase transition of $NaNiO_2$ in the voltage range below 3 V and above 4 V results in its main capacity loss during the first cycle, which was confirmed by high-energy XRD, synchrotron-based operando transmission X-ray microscopy, and GITT tests.⁹⁶ In general, increasing the reversibility of phase transformation or inhibiting irreversible phase transformation is the main research direction for layered $NaNiO_2$.

In 1982, layered $O3$ -type $NaCrO_2$ was found to show Na ion intercalation with about 120 mAh g^{-1} reversible capacity for the first time.⁹⁷ However, $LiCrO_2$ was indeed electrochemically inert as the cathode for LIBs due to the irreversible migration of Cr^{6+} into interstitial tetrahedron sites during the charge and discharge process.^{98,99} Instead, a similar process cannot occur in $NaCrO_2$ because of the size mismatch of Cr^{6+} and Na^+ .¹⁰⁰ Yang and coworkers revealed that layered $NaCrO_2$ goes through two-phase regions and three solid solution regions in turn during the whole charging process ($O3_R \leftrightarrow O3_R + O3_M \leftrightarrow O3_M \leftrightarrow P3_M + O3_M \leftrightarrow P3_M$).¹⁰¹ Myung et al. synthesized a carbon-coated $NaCrO_2$ cathode using an emulsion-drying method,²⁹ and it shows superior rate capability (99 mAh g^{-1} at 150 C) and excellent capacity retention (96% after the 50th cycle). Meanwhile, the carbon coating layer can prevent O loss from the crystal lattice to delay exothermic decomposition.

Generally, there are two types of Na_xVO_2 system: the $O3$ phase with the $R\bar{3}m$ space group and the $P2$ phase with the $P63/mmc$ space group.^{102–104} $O3-NaVO_2$ presents a reversible capacity of 120 mAh g^{-1} between 1.2 and 2.4 V, while $P2-Na_{0.7}VO_2$ shows only 105 mAh g^{-1} reversible discharge capacity.¹⁰⁵ Delmas and coworkers demonstrated that there are mainly four single-phase domains in the range of $0.5 \geq x \geq 0.9$.¹⁰⁶ The difference in sodium/vacancy ordering during the Na extraction process leads to commensurable or incommensurable superstructures. Although vanadium-based layered oxides present sufficient reversible capacity, their low-voltage platform hinders their development as cathodes for SIBs.

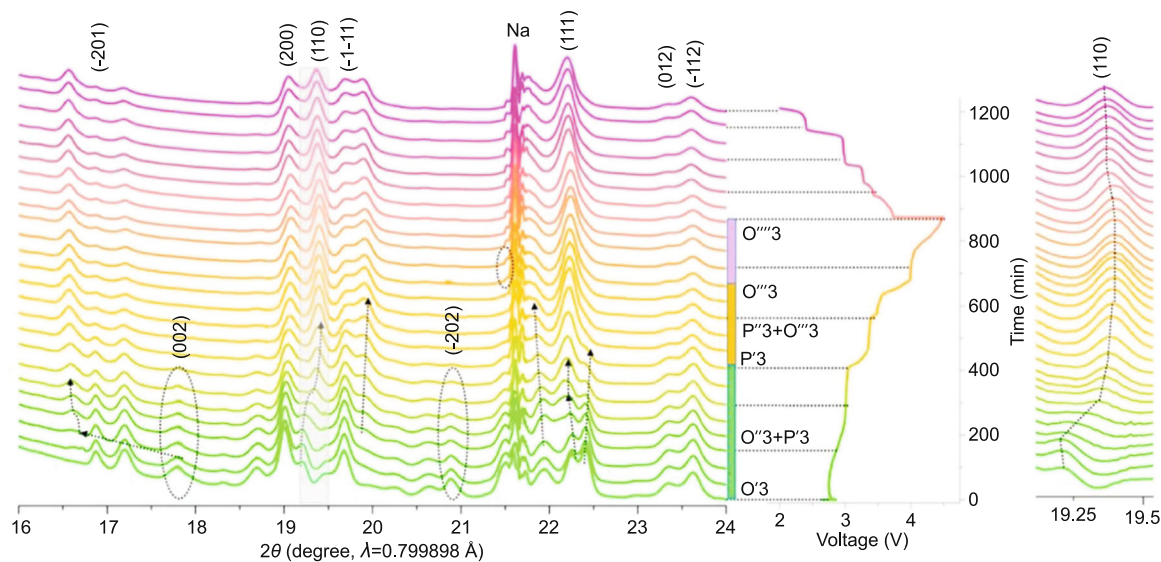


FIGURE 5 In situ synchrotron HE-XRD patterns of NaNiO_2 during the first cycle. Reproduced with permission: Copyright 2017, Elsevier⁹⁶

4.2 | Binary metal oxides

Although single-metal oxides present advantages, their insufficient comprehensive electrochemical performance limits their application. For example, layered Na_xMnO_2 has high specific discharge capacity, but its capacity attenuation is too severe to be a durable cathode electrode due to Jahn–Teller distortion of Mn^{3+} and irreversible phase transition. In this case, it is imperative to introduce another metal element to optimize the overall performance of the system. To build cost-effective batteries, design of multiple metal oxide cathodes with desirable cell performance is the general direction of future research. For example, the high-voltage redox couples such as $\text{Fe}^{3+}/\text{Fe}^{4+}$ and $\text{Ni}^{2+}/\text{Ni}^{4+}$ can improve the energy density and increase the operating voltage. Moreover, inert elements like Mg^+ and Li^+ can introduce oxygen reduction reactions to enhance reversible capacity, which will be described here.

Mn/Ni-based binary metal oxides are the most widely researched electrode materials owing to their high capacity and high operating voltage, which result from the synergistic action of Mn and Ni. $\text{P2-Na}_{1/3}\text{Ni}_{1/3}\text{Mn}_{2/3}\text{O}_2$ delivers a reversible capacity of 161 mAh g^{-1} with a 3.7 V average discharge voltage during 2–4.5 V.¹⁰⁷ The in situ XRD results demonstrate that $\text{Na}_x\text{Ni}_{1/3}\text{Mn}_{2/3}\text{O}_2$ retains the P2 phase when x is larger than 1/3, while it is partially transformed into the O2 phase leading to the coexistence of the two phases of P2 and O2 when x is smaller than 1/3. Pure O3- $\text{NaNi}_{0.66}\text{Mn}_{0.44}\text{O}_2$ synthesized via solid-state reactions presents a high discharge capacity of 190 mAh g^{-1} .¹⁰⁸ Komaba and coworkers investigated the structural transition mechanism of O3-type $\text{NaNi}_{0.5}\text{Mn}_{0.5}\text{O}_2$ with the $\text{R}\bar{3}\text{m}$ space

group via XAS.⁴⁵ The stacking sequence of MO_2 slabs gradually changed during Na extraction in the range of 2.2–3.8 V, and it transformed from the O3 phase into O'3, P3, P'3, and P''3 phases. Noticeably, the irreversible P2–O2 phase transition appeared when $\text{Na}_x\text{Mn}_{2/3}\text{Ni}_{1/3}\text{O}_2$ was charged up to 4.2 V, which resulted in significant capacity degradation from 95% to 95% after 10 cycles.⁴⁷ Besides, it was proposed that oxygen ions participate in charge compensation upon initial charge in the $\text{P2-Na}_{0.78}\text{Ni}_{0.23}\text{Mn}_{0.69}\text{O}_2$ cathode, which provides a wide plateau at high voltage.⁴⁵ The existence of an oxygen reduction reaction and the elimination of the P2–O2 phase transition contribute to the high reversible capacity and excellent cycling performances of $\text{Na}_{0.78}\text{Ni}_{0.23}\text{Mn}_{0.69}\text{O}_2$. Recently, Fan et al. reported $\text{P2-Na}_{2/3}\text{Ni}_{1/3}\text{Mn}_{2/3}\text{O}_2$ nanofibers with a distinctive hierarchical nanostructure of porous nanofibers (Figure 6A–C),¹⁰⁹ which shows a surprisingly high rate capacity and superior stability (109.9 mAh g^{-1} at 5 C with a capacity retention of 80.8% even after 500 cycles, as shown in Figure 6D). Density functional theory (DFT) computations show that the low ionic migration barrier and rapid reaction kinetics are responsible for the high rate capability. Overall, further development of Mn/Ni-based binary metal oxides should be considered to optimize their stability by improving the reaction power and alleviating the irreversible phase transition of P2–O2.

Significantly, partial substitution of cobalt can obviously improve the cycle stability of Mn-based metal oxides. Yamada and coworkers prepared $\text{P2-Na}_{2/3}\text{Mn}_y\text{Co}_{1-y}\text{O}_2$ via the conventional solid-state reaction,¹¹⁰ and they found that with the increase of the y value, its cycle stability degrades while the initial specific capacity increases. The

partial substitution of Co accelerates the formation of the passivating layer on the surface of Mn-based metal oxides. Besides, Srinivasan et al. proposed that the improved cycle stability of 10% Co-doped P2-Na_xCo_{0.1}Mn_{0.9}O₂ hollow spheres and hexagonal flakes is due to three effects: (1) suppression of the Jahn–Teller effect; (2) suppression of Na⁺ ordering processes; and (3) improvement of Na⁺ kinetics.¹¹¹ The P2-Na_{0.67}Co_{0.5}Mn_{0.5}O₂ with hierarchical architectures even shows 88 mAh g⁻¹ at a current density of 30 C with 50% capacity retention over 2000 cycles.¹¹² Meanwhile, research results show that the large active surface of (010)/(100) planes caused by the highly (001)-oriented nanosheets of the P2-Na_xCo_{0.7}Mn_{0.3}O₂ (*x* ≈ 1.0) cathode facilitates Na ion extraction/intercalation.¹¹³ In general, introducing Co element into layered Na_xMnO₂ oxides is conducive to the construction of a stable structure with fast Na⁺ kinetics and suppressed Na⁺ ordering.

Mn/Fe-based binary metal oxides are also receiving attention due to the abundant resources of both manganese and iron present in the Earth's crust. The discharge capacity of P2-Na_x[Fe_{1/2}Mn_{1/2}]O₂ reaches 190 mAh g⁻¹ with energy

density up to 520 mWh g⁻¹.¹¹⁴ The submicrometer-sized primary particles without a carbon coating show electrochemical activity, and their density (4.1 g cm⁻³) is higher than that of LiFePO₄ (3.6 g cm⁻³). In addition, Na_{2/3}(Fe_{1/2}Mn_{1/2})O₂ hierarchical nanofibers synthesized by electrospinning deliver enhanced cyclability compared with Na_{2/3}(Fe_{1/2}Mn_{1/2})O₂ nanoparticles.¹¹⁵ The good interconnection among the fibers promotes well-guided charge transfers and better electrolyte contact, which ensure an initial discharge capacity of 195 mAh g⁻¹. Rojo et al. investigated the phase composition and lattice parameters during electrochemical cycling of P2-Na_{2/3}Fe_{0.4}Mn_{0.6}O₂ through in situ XRD test.¹¹⁶ Increased interlayer distance in the charged state stabilizes the P2 structure and suppresses the formation of the highly disordered and unfavorable “Z” or OP4 phases. However, P'2 and two subtly different P2 phases were observed during the discharge state. Besides, air-stable Cu-doped P2-Na_{7/9}Cu_{2/9}Fe_{1/9}Mn_{2/3}O₂ with a high sodium content was reported as a cathode for SIBs by Chen's group,¹¹⁷ and it shows superior capacity retention of 85% over 150 cycles at

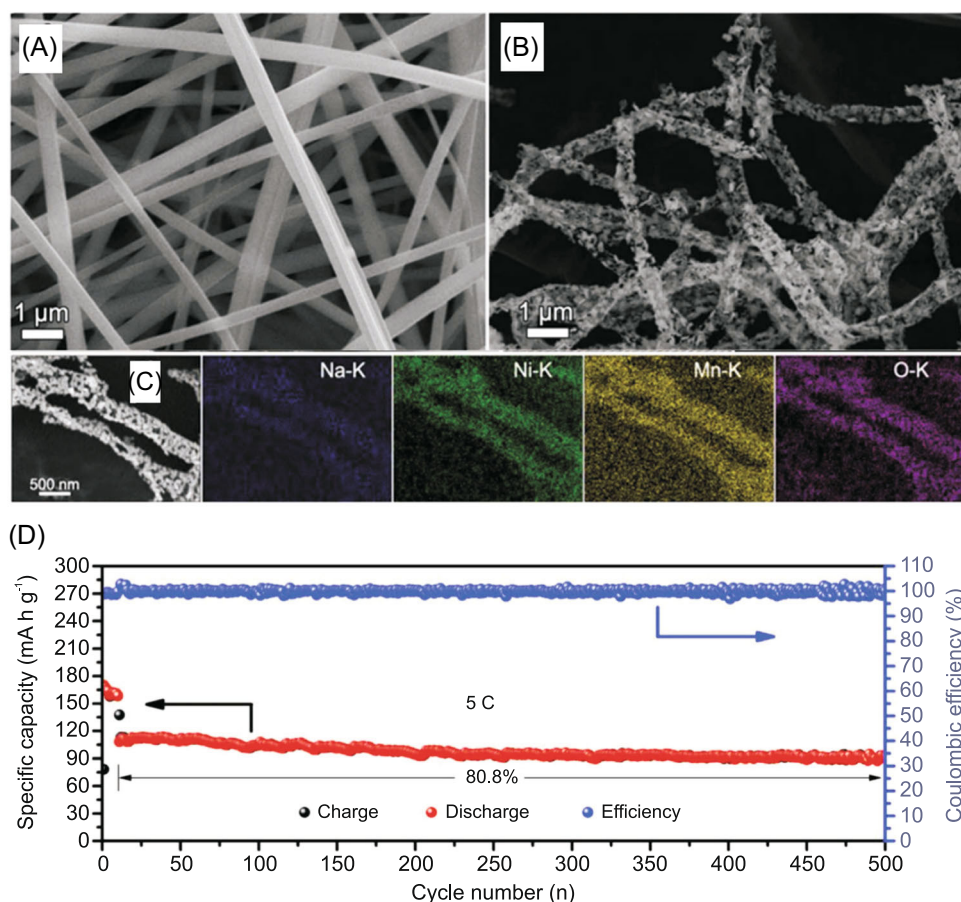


FIGURE 6 Scanning electron microscopy (SEM) images of (A) electrospun nanofibers and (B) resultant Na_{2/3}Ni_{1/3}Mn_{2/3}O₂ nanofibers; (C) energy-dispersive spectroscopy mapping images of the Na_{2/3}Ni_{1/3}Mn_{2/3}O₂ nanofibers; (D) long-term cycling life of the Na_{2/3}Ni_{1/3}Mn_{2/3}O₂ nanofibers at 5 C. Reproduced with permission: Copyright 2019, Wiley¹⁰⁹

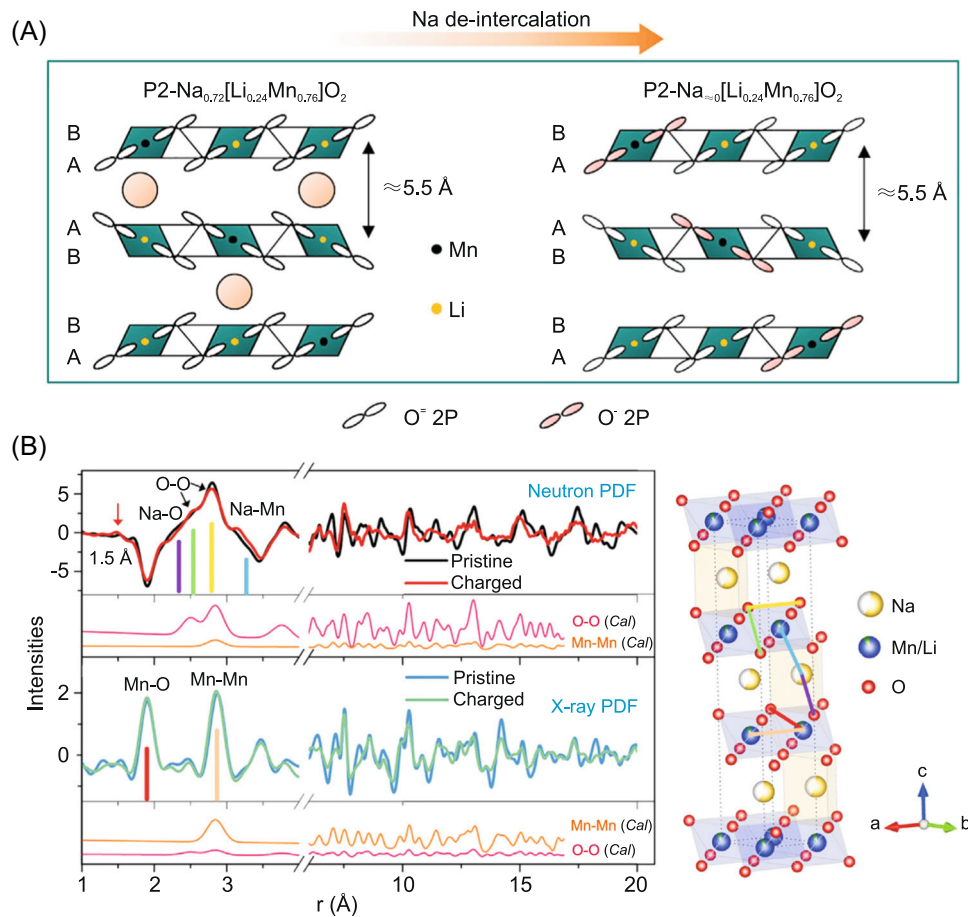


FIGURE 7 (A) Interaction of $\text{P2-Na}_{0.72}[\text{Li}_{0.24}\text{Mn}_{0.76}]\text{O}_2$ between the slabs when oxygen oxidation is involved. Reproduced with permission: Copyright 2019, Elsevier.⁶⁴ (B) X-ray and neutron pair distribution function (PDF) results of $\text{Na}_{0.6}[\text{Li}_{0.2}\text{Mn}_{0.8}]\text{O}_2$ collected at pristine and charged states (4.5 V). Reproduced with permission: Copyright 2017, Elsevier⁶⁰

1C without phase transition during the whole process. When coupled with a hard carbon anode, it delivers a high reversible capacity of 313 mAh g^{-1} with 79% initial Coulombic efficiency. Besides, a series of other metal-doped Mn/Fe-based oxides have also been extensively researched and have shown promising electrochemical performance, such as $\text{P2-Na}_{2/3}\text{Mn}_{0.8}\text{Fe}_{0.1}\text{Ti}_{0.1}\text{O}_2$,¹¹⁸ $\text{P2-Na}_{0.67}\text{Li}_{0.1}\text{Fe}_{0.4}\text{Mn}_{0.5}\text{O}_2$,¹¹⁹ $\text{O3-NaCo}_{1/3}\text{Fe}_{1/3}\text{Mn}_{1/3}\text{O}_2$,¹²⁰ and P2/O3 biphasic $\text{Na}_{0.67}\text{Fe}_{0.425}\text{Mn}_{0.425}\text{Mg}_{0.15}\text{O}_2$.¹²¹

Inactive metal substitution, especially Li substitution to induce the anion reduction reaction, has been extensively studied in Mn-based layered oxides. Chen et al. reported P2-type $\text{Na}_{0.72}[\text{Li}_{0.24}\text{Mn}_{0.76}]\text{O}_2$, which shows an ultrahigh reversible capacity of approximately 270 mAh g^{-1} between 1.5 and 4.5 V, corresponding to more than 700 Wh kg^{-1} energy density.⁶⁴ To date, this is the highest discharge capacity and energy density compared with other previously reported materials used in cathodes of SIBs. A pure anionic redox reaction process ensures such a high capacity, and consequent suppression of the phase transition leads to minimal volume change (1.35%), with no decrease in the interslab

distance on completely removing Na (Figure 7A). Besides, Nazar and coworkers proved that $\text{P2-Na}_{0.6}\text{Li}_{0.2}\text{Mn}_{0.8}\text{O}_2$ also shows a high specific capacity of up to 190 mAh g^{-1} .¹²² The DFT calculations indicate that the energy states of oxygen are located near the Fermi level, demonstrating participation of oxygen in the redox process. The introduction of lithium improves the stability of the structure by inhibiting the harmful irreversible phase transition. In the meantime, the oxygen 2p orbital at the top of the valence band results in the formation of O_2 gas.¹²³ Similarly, $\text{Na}(\text{Li}_{1/3}\text{Mn}_{2/3})\text{O}_2$ designed on the basis of first-principles calculations shows high redox potentials ($\approx 4.2 \text{ V}$) and high charge capacity (190 mAh g^{-1}) due to an anionic redox reaction (O^{2-}/O^-).¹²⁴ Li in the transition-metal layers is the key to this wide range of Na intercalation.¹²⁵ P3-type $\text{Na}_{0.6}[\text{Li}_{0.2}\text{Mn}_{0.8}]\text{O}_2$ is reported to be a promising cathode material with outstanding electrochemical performances through an anionic redox reaction.⁶⁰ The oxidation of oxygen anions resulted in the shortening of the O–O distance to 2.5 \AA , which was detected by the neutron total scattering technique, as shown in Figure 7B. Such an O–O dimer is stabilized in the cationic

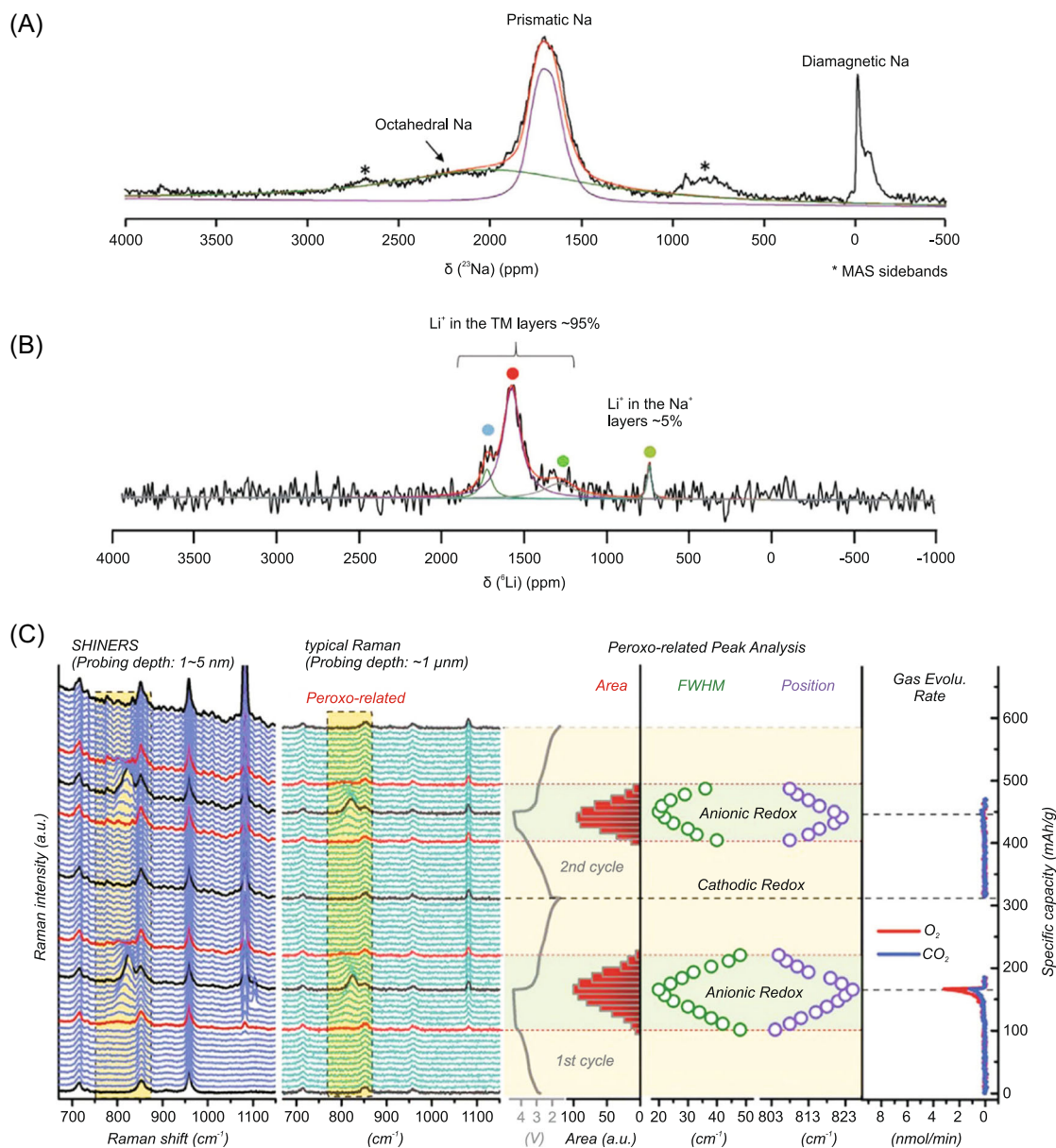


FIGURE 8 Magic angle spinning (MAS) solid-state NMR spectra of (A) ^{23}Na and (B) ^6Li (B) for $\text{Na}_{0.8}\text{Li}_{0.2}\text{Fe}_{0.2}\text{Mn}_{0.6}\text{O}_2$. *MAS rotational side bands. The groups of signals marked with blue, red, and green spots are assigned to Li ions at TM layers close to Fe and/or Mn, whereas the light green dot indicates Li in Na layers. Reproduced with permission: Copyright 2020, Wiley.¹²⁶ (C) Additional insight into oxygen-centered processes. In situ SHINERS and in situ bulk Raman spectra during the first and second cycles, as well as the corresponding in situ DEMS results of the gas evolution rate. Area and FWHM as well as the position of the peroxy-related peak represented from the in situ spectra. Reproduced with permission: Copyright 2020, Wiley¹²⁷

network by strong metal–oxygen covalent bonding. In addition, weakened Mn–O covalent bonding plays a crucial role in stabilizing the oxidized oxygen species (Figure 7B). For future investigation of the charge compensation mechanism and phase transformation mechanism of Na_xTMO_2 , the development and usage of advanced characterization methods and theoretical analysis are also significant for frontier research. Philipp et al. used solid-state nuclear magnetic resonance (ssNMR)

spectroscopy to explore the Li^+ occupation during cycling, and they revealed that 5% Li^+ migrated from the TM to the alkali layers in the first charge as shown in Figure 8A,B.¹²⁶ This phenomenon confirmed a widely accepted theory that in the host lattice, at a relatively high voltage, the inactive elements removed from the lattice leave plenty of vacancies that can trigger the O redox reaction.

To improve the storage capacity of sodium and enhance the stability of materials, Mn/Mg binary oxides are

designed. As the increase content of magnesium ions in the host structure, P2-type $\text{Na}_{2/3}[\text{Mg}_{0.28}\text{Mn}_{0.72}]\text{O}_2$ presents a surprising discharge capacity of 220 mAh g^{-1} .¹²⁸ Large capacity is considered to promote the participation of oxygen ions in the redox reaction. Meanwhile, it was found that a small amount of Mg doping ($\approx 5\%$) is conducive to smoothing the charge and discharge profiles without reducing the capacity and improving cycling stability.¹²⁹ Bruce's group reported that the oxygen redox reaction in P2- $\text{Na}_{2/3}[\text{Mg}_{0.28}\text{Mn}_{0.72}]\text{O}_2$ occurs in oxygen $2p$ orbitals, which interact with alkali metal ions in the transition-metal layer.⁵⁹ Unlike the alkali-rich compounds, there is no oxygen loss during the charge process. For P3-type $\text{Na}_{0.6}[\text{Li}_{0.2}\text{Mn}_{0.8}]\text{O}_2$ with a weak Mn–O covalent bond, Mg plays an important role in stabilizing the oxidation state and inhibiting the irreversible change of oxidation products to O_2 gas.⁶⁰ In addition, the reversible anionic redox chemistry has been detected by in situ SHINERS and in situ bulk Raman spectra as shown in Figure 8C.¹²⁷ Advanced characterization techniques revealed the evolution process of lattice oxygen, peroxy/superoxo-like species, and O_2 during the initial Na^+ desodiation activation. More importantly, reversible anionic and cationic redox reaction have been achieved simultaneously, while no irreversible oxygen behaviors can be observed.

The copper-doped sodium ion manganese oxides have been extensively studied in phase transition-free cathodes for SIBs. Kim et al. prepared $\text{Na}_{2.3}\text{Cu}_{1.1}\text{Mn}_2\text{O}_{7-d}$ nanoflakes using an ultrafast pyrosynthesis process.¹³⁰ Superior structural stability was achieved at 20 C (72.4 mAh g^{-1} with 88% capacity retention after 900 cycles), which was attributed to the single-phase reaction during the Na^+ extraction/insertion process and the nanoflake morphology. Interestingly, layered $\text{Na}_{0.67}\text{Cu}_{0.28}\text{Mn}_{0.72}\text{O}_2$ shows reversible lattice oxygen redox activity with slight voltage hysteresis.⁴⁰ The nonbonding oxygen $2p$ states in the Cu–O bonds guarantee the oxygen redox activity, and there is no phase transition during electrochemical cycling. The stable oxygen stacking sequence promotes the smoothing of the voltage profile. In addition, P2- $\text{Na}_{2/3}\text{Mn}_{7/9}\text{Zn}_{2/9}\text{O}_2$ shows anionic redox activity without O_2 release due to the introduction of high electronegative elements, and it also delivers a reversible discharge capacity of 200 mAh g^{-1} in the Na half-cell and 140 mAh g^{-1} in the full-cell.¹³¹ Moreover, it was found that a small amount of Al doping in Mn-based oxides contributes to the improvement of electrochemical properties due to the suppression of the Jahn–Teller distortion of Mn^{3+} and the enhancement of the Na-diffusion coefficient.¹³² To sum up, inactive doping in Mn-based oxides is very important for the triggering of the anionic redox reaction, stabilization of the phase structure, and the improvement of material dynamic properties.

Honeycomb-layered metal oxides $\text{Na}_3\text{M(II)}_2\text{M(V)}\text{O}_6$, where M represents cations, are considered to be promising candidates as cathodes for SIBs. Each $\text{M(V)}\text{O}_6$ octahedron is surrounded by six $\text{M(II)}\text{O}_6$ octahedra in plane, corresponding to the space group of $C2/m$. Because of the significant size difference between M(II) and M(V) , cations are arranged in an orderly manner in the transition-metal layers to form a honeycomb structure. Highly ordered honeycomb-layered $\text{Na}_3\text{Ni}_2\text{BiO}_6$ with a monoclinic superstructure can deliver an initial discharge capacity of 109 mAh g^{-1} .¹³³ Two reversible phase transitions ($\text{O3} \leftrightarrow \text{P3} \leftrightarrow \text{O1}$) were found via operando XRD studies in the charge–discharge process. Besides, $\text{O3-Na}_3\text{Ni}_2\text{SbO}_6$ prepared by a high-temperature solid-state reaction with the space group $C2/m$ shows $122/117 \text{ mAh g}^{-1}$ charge/discharge capacity at a narrow potential interval of $3.8\text{--}3.1 \text{ V}$.¹³⁴ Khalifah and coworkers investigated the different structures of O3-type $\text{Na}(\text{Ni}_{2/3}\text{Sb}_{1/3})\text{O}_2$ ($R\bar{3}m$ for the disordered structure and $C2/m$ for the ordered variant).¹³⁵ It is found that the disordered $\text{Na}(\text{Ni}_{2/3}\text{Sb}_{1/3})\text{O}_2$ ordered honeycomb structure can be better used to describe this structure, and NMR results show that it is difficult to distinguish honeycomb ordering of Ni and Sb cations in the transition-metal layers from the ordered phase. The full theoretical discharge capacity for the ordered variant can reach 133 mAh g^{-1} , while that of disordered materials can only reach 110 mAh g^{-1} . Recently, Guo et al. demonstrated that the construction of a honeycomb-type superlattice in the layered metal oxides shows an ultralong charge/discharge plateau and a structural transition without cation migration.¹³⁶ They designed and synthesized $\text{Na}_3\text{Ni}_2\text{RuO}_6$ with a transition-metal-ordered superlattice structure, and finally, $\text{Na}_3\text{Ni}_2\text{RuO}_6$ achieved a superlong potential plateau, high reversible specific capacity, and excellent cycle performance.

To overcome the Jahn–Teller distortion of the trivalent Ni, cation doping is considered an effective strategy. O3-type $\text{NaTi}_{0.5}\text{Ni}_{0.5}\text{O}_2$ delivered 121 mAh g^{-1} reversible capacity with an average potential of 3.1 V at a current of 0.2 C .¹³⁷ Reversible O3–P3 transformation was found, and Ti remained inactive in the potential window of $1.5\text{--}4.2 \text{ V}$.¹³⁸ A similar O3–P3 phase transition was also observed in $\text{NaNi}_{0.5}\text{Co}_{0.5}\text{O}_2$ and $\text{NaNi}_{0.5}\text{Fe}_{0.5}\text{O}_2$.¹³⁹ The combination of Fe and Ni not only inhibits the polarization but also suppresses the Jahn–Teller effect of Ni^{3+} during the charge/discharge process.

4.3 | Ternary metal oxides

Na_xMO_2 cathodes with a single metal and binary metal show unique advantages; however, the structure

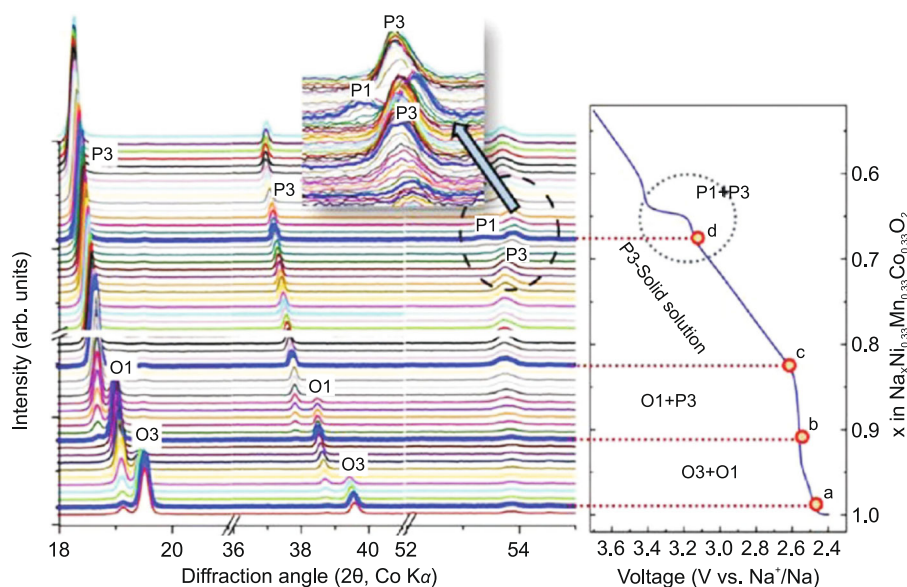


FIGURE 9 In situ X-ray diffraction patterns recorded during the initial charge for a $\text{NaNi}_{1/3}\text{Mn}_{1/3}\text{Co}_{1/3}\text{O}_2$ electrode. Reproduced with permission: Copyright 2012, American Chemical Society¹⁴⁷

degenerates rapidly due to the existence of a phase transition in the process of Na^+ deintercalation/intercalation, which hinders their development. Introduction of an inactive metal into transition-metal oxide layers can be an effective modification method.¹⁴⁰ It is found that the P2–O2 phase transition is significantly mitigated in layered $\text{Na}_{0.67}\text{Mn}_{0.67}\text{Ni}_{0.33-x}\text{Mg}_x\text{O}_2$ ($0 \leq x \leq 0.33$).¹⁴¹ The prepared P2- $\text{Na}_{0.67}\text{Mn}_{0.67}\text{Ni}_{0.28}\text{Mg}_{0.05}\text{O}_2$ shows an initial capacity of 123 mAh g^{-1} with a high-energy density of 455 Wh kg^{-1} (vs. Na^+/Na). Inactive Mg^{2+} in transition-metal oxide layers stabilizes the total charge balance of compounds, and more Na^+ ions reside in prismatic sites upon charging. Bruce et al. have investigated the effects of magnesium substitution on the structure, electrochemical properties, and Na^+ ion diffusion of P2-type $\text{Na}_{2/3}\text{Ni}_{1/3-x}\text{Mg}_x\text{Mn}_{2/3}\text{O}_2$ ($0 \leq x \leq 0.2$) in the high-voltage range.¹⁴² The results of neutron diffraction show that Mg^{2+} replaces Ni^{2+} in ordered $[(\text{Ni}^{2+}/\text{Mn}^{4+})\text{O}_6]$ honeycomb units. Excessive Mg substitution leads to the disorder of Na distribution rather than typical Na zig-zag ordering. Furthermore, DFT calculation also confirm the improvement of Na-ion diffusion ability. Besides, Ti-substituted O3-type $\text{NaNi}_{0.5}\text{Mn}_{0.2}\text{Ti}_{0.3}\text{O}_2$ was successfully synthesized by a solid-phase reaction.¹⁴³ Partial Ti substitution could maintain a highly reversible O3–P3 phase transition in a large voltage regions, resulting in high reversible discharge capacity (135 mAh g^{-1}) and good capacity retention ($\approx 85\%$ at 1 C after 200 cycles). Ternary metal oxides doped with other inactive metals (such as Al, Zn, Zr, etc.) have also been widely investigated.^{118,144–148}

To obtain excellent cathode materials with all-round comprehensive properties, different $\text{Na}_x[\text{Mn Ni Co}]\text{O}_2$

cathodes were prepared. A layered $\text{NaNi}_{1/3}\text{Mn}_{1/3}\text{Co}_{1/3}\text{O}_2$ compound was successfully synthesized using the sol–gel method, which delivered an initial capacity of 120 mAh g^{-1} .¹⁴⁹ During Na insertion/deinsertion, $\text{NaNi}_{1/3}\text{Mn}_{1/3}\text{Co}_{1/3}\text{O}_2$ forms biphasic and monophasic domains caused by phase transitions. As shown in Figure 9, the phase evolution in $\text{NaNi}_{1/3}\text{Mn}_{1/3}\text{Co}_{1/3}\text{O}_2$ follows the sequence of O3–O1–P3–P1, which is revealed by in situ XRD patterns. Besides, it is found that $\text{NaNi}_{1/3}\text{Mn}_{1/3}\text{Co}_{1/3}\text{O}_2$ is unstable in air, resulting in a nonstoichiometric $\text{Na}_x\text{Ni}_{1/3}\text{Mn}_{1/3}\text{Co}_{1/3}\text{O}_2 \cdot \text{H}_2\text{O}$ hydrated phase. Wang et al. used first-principles calculations to predict the structural stability, electronic structures, and diffusion barrier.¹⁵⁰ The d-electron configurations of Ni, Co, and Mn in $\text{NaNi}_{1/3}\text{Co}_{1/3}\text{Mn}_{1/3}\text{O}_2$ are $\text{Ni}(t_{2g})^6(e_g)^2$, $\text{Co}(t_{2g})^6(e_g)^0$, and $\text{Mn}(t_{2g})^3(-e_g)^0$, respectively. The Ni^{2+} and Mn^{4+} , which do not undergo Jahn–Teller distortion, can reinforce the structural stability. Based on the superlattice model, the calculations of the solid-state redox reaction in the process of Na^+ deintercalation show that $\text{Ni}^{2+}/\text{Ni}^{3+}$, $\text{Ni}^{3+}/\text{Ni}^{4+}$, and $\text{Co}^{3+}/\text{Co}^{4+}$ in $\text{Na}_x\text{Ni}_{1/3}\text{Co}_{1/3}\text{Mn}_{1/3}\text{O}_2$ correspond to the Na contents of $2/3 \leq x \leq 1$, $1/3 \leq x \leq 2/3$, and $0 \leq x \leq 1/3$, respectively. At room temperature, its Na^+ migration is 10 times faster than that of pristine layered NaCoO_2 , which is attributed to the lower diffusion barrier. Furthermore, the role of Co has been comprehensively investigated by Liu et al.¹⁵¹ Compared with Co-free $\text{Na}_{0.7}\text{Mn}_{0.7}\text{Ni}_{0.3}\text{O}_2$, $\text{Na}_{0.7}\text{Mn}_{0.7}\text{Ni}_{0.2}\text{Co}_{0.1}\text{O}_2$ and $\text{Na}_{0.7}\text{Mn}_{0.7}\text{Ni}_{0.1}\text{Co}_{0.2}\text{O}_2$ show higher rate capability and better cycle performance. With the introduction of Co^{3+} , the lattice parameter c increases and a decreases. In addition, due to the smaller radius of Co^{3+} than that of Ni^{2+} , Co substitution

enhances the diffusion coefficient of Na⁺ ions and shortens the lengths of M–O and O–O bonds, which leads to shrinkage of the volume of the MO₆ octahedron. The contraction of the MO₆ octahedron promotes the structural stability and cycle performance. Last but not the least, electronic conductivity can also be improved by the aliovalent substitution of Co³⁺, which contributes to the improvement of rate performance.

Since Cu has been shown to be electrochemically active in layered oxide materials for SIBs, Cu is widely used for doping into the P2-Na_{2/3}Ni_{1/3}Mn_{2/3}O₂ system, which is an important modification method. Air-stable Na_{2/3}Ni_{1/4}Cu_{1/12}Mn_{2/3}O₂, Ni²⁺/Ni³⁺, Ni³⁺/Ni⁴⁺, and Cu²⁺/Cu³⁺ redox reactions during cycling confer it with a high operating voltage and high specific capacity.¹⁵² It retains the P2/OP4 structure even when charged to high voltages. Phase changes were suppressed due to the introduction of Cu, resulting in an excellent capacity retention. Cao et al. successfully synthesized P2-type Na_{0.67}Ni_{0.1}Cu_{0.2}Mn_{0.7}O₂ for SIBs via the sol-gel method.⁵³ Compared with the Na_{0.67}Ni_{0.3}Mn_{0.7}O₂ electrode, Na_{0.67}Ni_{0.1}Cu_{0.2}Mn_{0.7}O₂ delivers a better capacity retention. Copper substitution optimizes the structure of MO₂ layers, which suppresses the P2–O2 phase transition and Na⁺/vacancy ordering transition, as shown in Figure 9. Furthermore, the existence of divalent copper is conducive to increasing the capacity when charged to high voltage through the high potential Cu²⁺/Cu³⁺ redox. Moreover, Cao et al. have prepared pure P2-type Na_{0.67}Mn_{0.65}Fe_{0.2}Ni_{0.15}O₂ via the sol-gel method, which shows a high reversible specific capacity of 208 mAh g⁻¹ with 71% capacity retention over 50 cycles.⁵¹ Ex situ XRD patterns of the Na_{0.67}Mn_{0.65}Fe_{0.2}Ni_{0.15}O₂ electrode reveal a reversible two-phase transformation during Na⁺ deintercalation/intercalation. Among them, honeycomb-layered Na₃Ni_{1.5}M_{0.5}BiO₆ (M = Ni, Cu, Mg, Zn) has also been demonstrated to be a promising cathode.¹⁵³ Owing to the Ni²⁺/Ni³⁺ and Cu²⁺/Cu³⁺ redox couples, Na₃Ni_{1.5}Cu_{0.5}BiO₆ shows a considerably high capacity of 94 mAh g⁻¹ and high average voltage of 3.3 V. The M²⁺ (M = Cu, Mg, Zn) cations in Na₃Ni_{1.5}M_{0.5}BiO₆ not only stabilize the P'3 structure but also suppress the P'3–O1 phase transition, leading to a smooth electrochemical curve with high operating voltage. However, the electrochemical irreversibility increases during the discharge process in the substituted material, which may be the result of both the breaking of charge balance and the structural strain. Mn-rich P2-Na_{2/3}Mn_{0.8}Fe_{0.1}Ti_{0.1}O₂ synthesized by a ceramic method also shows stable electrochemical performance.¹¹⁸ The ssNMR results of Na confirm the substitution of Fe and Ti at the sites of Mn in the transition-metal oxide layer and fast mobility of Na⁺. The electrode shows a reversible discharge capacity of 144.16 mA h g⁻¹ with a retention of 95.09% after 50 cycles at 0.1 C. In addition, the reversible specific capacity

still remains 99.40 mAh g⁻¹ at 1 C, and a retention of 87.70% after 300 cycles is achieved.

Depending on the Na⁺ concentration, P2-type layered oxides usually show multiple single-phase domains accompanied by various Na⁺/vacancy-ordered superstructures. These superstructures promote the formation of multiple voltage plateaus and poor electrochemical performance as cathodes for SIBs. Guo et al. constructed a completely disordered Na vacancy in the Na layer to solve this problem.¹¹⁸ They prepared Ti-substituted P2-Na_{2/3}Ni_{1/3}Mn_{1/3}Ti_{1/3}O₂ to prevent electron delocalization and constructed a completely disordered arrangement of Na vacancy. A high Na⁺ mobility (10⁻¹⁰ to 10⁻⁹ cm² s⁻¹) and low activation energy barriers (170 meV) are achieved in the Na layers, resulting in smooth charge/discharge curves. The electrochemical performance test results show that Na_{2/3}Ni_{1/3}Mn_{1/3}Ti_{1/3}O₂ delivers an 83.9% capacity retention rate at 1 C after 500 cycles and 77.5% of the initial capacity at 20 C. Moreover, introduction of Mg into P2-type Na_{0.7}[Mn_{0.6}Ni_{0.4}]O₂ can also be an effective strategy to decrease Na⁺/vacancy-order superstructures.¹⁵⁴ Mg ions occupy both Na sites and transition-metal sites to generate “Na–O–Mg” and “Mg–O–Mg” configurations, leading to an ionic oxygen 2p character. The oxygen 2p orbital is located at the top of the O-valence band interacting with transition metals, inducing the occurrence of reversible oxygen reduction. The designed Na_{0.7}Mg_{0.05}[Mn_{0.6}Ni_{0.2}Mg_{0.15}]O₂ shows a smooth voltage distribution curve and a stable structure (Figure 10A,B). After charging, a new P2 phase, instead of the O2 phase, was found in Na_{0.7}Mg_{0.05}[Mn_{0.6}Ni_{0.2}Mg_{0.15}]O₂ in unsubstituted material. Several intermediate phases were observed during high-rate charge (Figure 10C), which is different from low-rate charge. The elemental-related redox couples and structural reorganization caused by the introduction of Mg affect Na-ion transport kinetics.

Most of the layered oxide cathodes undergoing oxygen reduction may undergo an irreversible electrochemical reaction and O₂ release, resulting in rapid capacity degradation. Strong electronegative copper can stabilize the P2-Na_{2/3}Mn_{0.72}Cu_{0.22}Mg_{0.06}O₂ with a sodium-deficient structure to achieve the reversible cationic and anionic redox reduction.¹⁵⁵ Mn³⁺/Mn⁴⁺, Cu²⁺/Cu³⁺, and O²⁻/(O²⁻)ⁿ⁻ all participate in the redox reaction during Na⁺ extraction/insertion. The strong covalency between copper and oxygen promotes the cationic and anionic redox activity. The P2-Na_{2/3}Mn_{0.72}Cu_{0.22}Mg_{0.06}O₂ shows stable cycle performance with a retention of 87.9% after 100 cycles at 1 C as well as excellent rate performance of 70.3 mAh g⁻¹ at 10 C. Furthermore, P2-Na_{0.66}Li_{0.22}Ti_{0.15}Mn_{0.63}O₂ was developed as a promising cathode, which combines cationic and anionic redox activities.¹⁵⁶ With the suppression of oxygen loss and the Mn³⁺/Mn⁴⁺ redox reaction, Jahn–Teller distortion and irreversible O₂ evolution are also effectively

restrained in the Ti-substituted layered $\text{Na}_{0.66}\text{Li}_{0.22}\text{Ti}_{0.15}\text{Mn}_{0.63}\text{O}_2$. Ti substitution in the layered oxide cathode has been confirmed to be an effective strategy to regulate the cationic and anionic redox activities.

The phase transformation at high voltage (>4.3 V vs. Na/Na^+) and the dissolution of active species in the electrolyte lead to the rapid degradation of the layered oxide cathodes, which hinders their application. It is crucial to design a reasonable interface modification strategy to obtain stable high-voltage SIBs. Ion-conductive polyimide (PI) encapsulation was used to improve the electrochemical performance of $\text{P2-Na}_{2/3}(\text{Mn}_{0.54}\text{Ni}_{0.13}\text{Co}_{0.13})\text{O}_2$ by Kaliyappan et al.¹⁵⁷ The PI-coated $\text{P2-Na}_{2/3}(\text{Mn}_{0.54}\text{Ni}_{0.13}\text{Co}_{0.13})\text{O}_2$ cathode delivered excellent cycle stability with a retention of 82% after 100 cycles at 0.16 A g^{-1} between 2.0 and 4.5 V, compared to that of Al_2O_3 -coated $\text{P2-Na}_{2/3}(\text{Mn}_{0.54}\text{Ni}_{0.13}\text{Co}_{0.13})\text{O}_2$ (70%) and the pristine (46%). It even demonstrated 70% capacity retention after 500 cycles at a high current density of 5 C. The ultrathin PI layer offers excellent surface protection, facile ion transport, and high ionic conductivity. Besides, carbonized polydopamine-derived (C-PDA) coating on P2-type $\text{Na}_{0.80}\text{Ni}_{0.22}\text{Zn}_{0.06}\text{Mn}_{0.66}\text{O}_2$ can yield higher discharge capacity, better rate capability, and better cycling

stability.¹⁵⁸ C-PDA prevents the deposition of $\text{Na}_2\text{CO}_3/\text{NaOH}$, which is advantageous to forming the cathode electrolyte interphase layer. Furthermore, the dual-modification strategy of $\text{NaTi}_2(\text{PO}_4)_3$ surface coating and Mg substitution for transition metals was designed to inhibit both the surface side reaction and phase transformation.¹⁵⁹ The NASICON-type $\text{NaTi}_2(\text{PO}_4)_3$ coating layer plays an important role in stabilizing the interface, preventing the impact of HF, and promoting the migration of Na^+ . In addition, the dual-modification strategy can also restrain particle crack and exfoliation. The dual-modification P2-type $\text{Na}_{0.67}\text{Ni}_{0.33}\text{Mn}_{0.67}\text{O}_2$ shows a capacity retention of 77.4% after 200 cycles at 1 C and excellent rate performance (106.8 mAh g^{-1} at 5 C). In conclusion, surface coating is a feasible strategy to design and modify high-performance layered oxides for SIBs.

O3-type oxides often suffer from the problems of a narrow operation voltage window and low reversible capacity. Hwang et al.¹⁶⁰ presented a cathode with varied chemical composition from the inner end ($\text{Na}[\text{Ni}_{0.75}\text{Co}_{0.02}\text{Mn}_{0.23}]\text{O}_2$) to the outer end ($\text{Na}[\text{Ni}_{0.58}\text{Co}_{0.06}\text{Mn}_{0.36}]\text{O}_2$), showing a radially aligned hierarchical columnar structure in spherical particles. It delivers a discharge

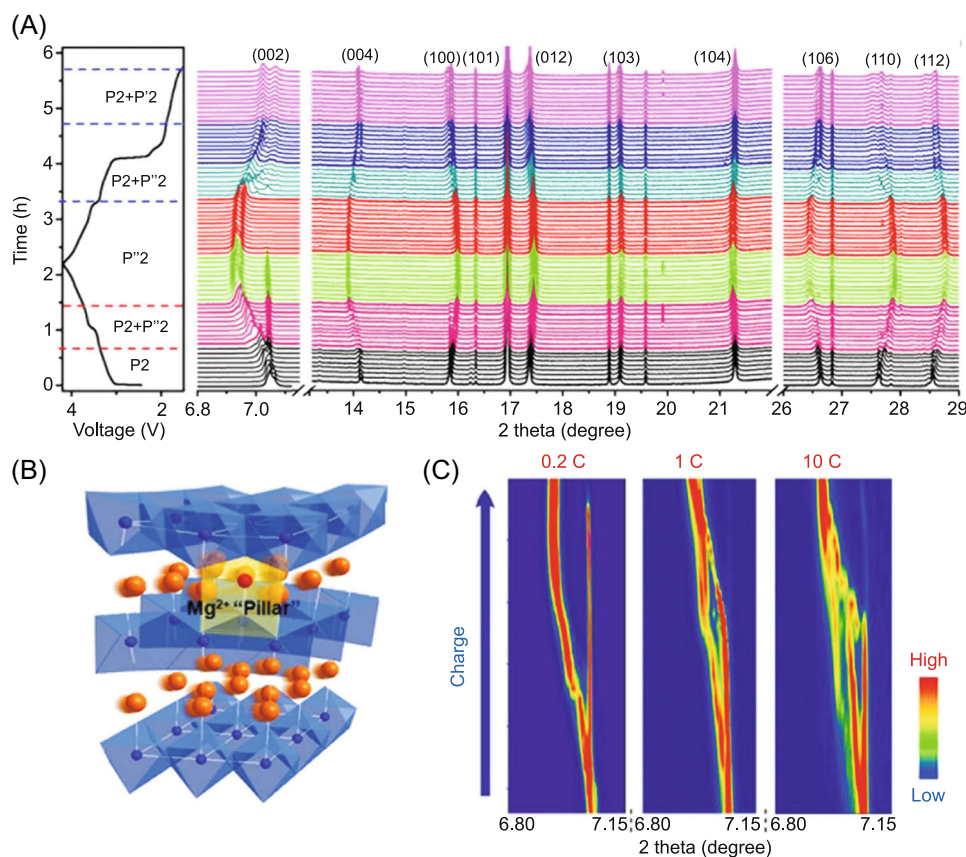


FIGURE 10 (A) Crystal structure evolution of $\text{P2-Na}_{0.7}\text{Mg}_{0.05}[\text{Ni}_{0.2}\text{Mn}_{0.6}\text{Mg}_{0.15}]\text{O}_2$. (B) The “pillars” function of Mg ions in the Na layer stabilize the layered structure. (C) Contour plot of the (002) peak evolution in the initial charge at various C rates (0.2, 1, and 10 C). Reproduced with permission: Copyright 2018, American Chemical Society¹⁵⁴

capacity of 157 mAh g^{-1} at a current density of 15 mA g^{-1} based on the electrochemical reaction of $\text{Ni}^{2+/3+/4+}$. They further used this cathode and hard carbon anode to obtain a full-cell, which not only shows excellent stability with 80% (125 mAh g^{-1}) retention after 300 cycles and excellent rate capability of 132.6 mAh g^{-1} at 10 C but also shows excellent low-temperature performance at -20°C . The unique chemistry of this cathode minimizes the contact of the surface area with the corrosive electrolyte and enables the Ni redox reaction. Meanwhile, a composition-graded layered oxide cathode with an average composition of $\text{Na}[\text{Ni}_{0.61}\text{Co}_{0.12}\text{Mn}_{0.27}]\text{O}_2$ was synthesized by Sun et al., and it showed outstanding performance and stability.¹⁶¹ Compared with constant-concentration (CC) $\text{Na}[\text{Ni}_{0.61}\text{Co}_{0.12}\text{Mn}_{0.27}]\text{O}_2$ (Figure 11A), composition-graded $\text{Na}[\text{Ni}_{0.61}\text{Co}_{0.12}\text{Mn}_{0.27}]\text{O}_2$ is a spherical particle assembled by many spoke-like nanorods, and the concentration of transition metals inside shows a gradient distribution (Figure 11B). As shown in Figure 11C,D, individual nanorods show strong crystallographic texture and microcompression tests confirm its mechanical robustness. This morphology can minimize the porosity and improve the mechanical strength of the particles, while promoting the transport of Na^+ into the particles. This hierarchical columnar $\text{Na}[\text{Ni}_{0.61}\text{Co}_{0.12}\text{Mn}_{0.27}]\text{O}_2$ delivers a high reversible specific capacity of 160 mAh g^{-1} at 15 mA g^{-1} and up to 130 mAh g^{-1} at 10 C.

4.4 | Multiple metal oxides

To improve the comprehensive properties of layered Na_xMO_2 cathodes, an efficient strategy is to introduce multiple metal ions into a transition-metal site, so as to

optimize the structure and obtain better electrochemical properties. Minor quantities of Cu, Mg, Li, Ti, Fe, and so forth, are introduced into oxide compounds to form novel four or more transition-metal oxides with unique properties.

O3-type layered $\text{Na}(\text{Mn}_{0.25}\text{Fe}_{0.25}\text{Co}_{0.25}\text{Ni}_{0.25})\text{O}_2$ (MFCN) synthesized via a solid-state method delivers an initial discharge capacity of 180 mAh g^{-1} and high energy density up to 578 Wh kg^{-1} with excellent cycling performance at a high-voltage range.¹⁶² The evolution of an O3-P3-O3'-O3'' reversible structure was found during Na^+ deintercalation/intercalation by in situ XRD, as shown in Figure 12A. The number of active Jahn-Teller ions in MFCN is much lower than that in the $\text{Na}(\text{Ni}_{0.5}\text{Mn}_{0.5})\text{O}_2$ (NM) system, with only 25% Ni in the MFCN cathode compared with 50% in the NM cathode. A quaternary O3-type $\text{NaCr}_{1/4}\text{Fe}_{1/4}\text{Ni}_{1/4}\text{Ti}_{1/4}\text{O}_2$ (NCFNT) layered material was investigated as a cathode for SIBs by Cao et al.¹⁶³ NCFNT shows a discharge capacity of 129.2 mAh g^{-1} at 0.1 C, with 95.4% Coulombic efficiency, and it also shows excellent capacity retention of 77.1% after 300 cycles at 1 C. Irreversible phase transformation and the irreversible redox of $\text{Cr}^{3+}/\text{Cr}^{6+}$ during Na^+ deintercalation/intercalation are the fundamental reasons for capacity decay in the initial cycle, which is confirmed by ex situ XRD and XAS results.

Ti-contained multimetal oxide cathodes with a stable structure are extensively studied. A small amount of Ti-doped O3- $\text{Na}[\text{Ti}_x(\text{Ni}_{0.6}\text{Co}_{0.2}\text{Mn}_{0.2})_{1-x}]\text{O}_2$ was found to be a high-performance cathode material for SIBs.¹⁶⁵ After Ti doping, the primary particles aggregate to form denser secondary particles, resulting in high tap density ($\sim 2.3 \text{ g cm}^{-3}$) and enhanced mechanical strength. Compact particles effectively avoid unwanted side effects by reducing the volume of voids that can penetrate the

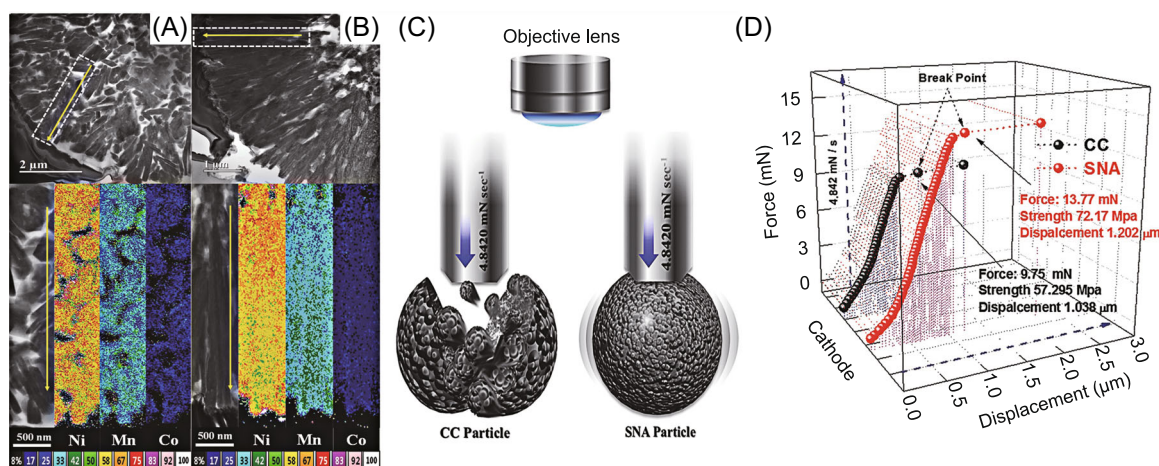


FIGURE 11 Cross-sectional TEM images and the corresponding EDAX mapping (selected area) of (A) constant-concentration (CC) $\text{Na}[\text{Ni}_{0.61}\text{Co}_{0.12}\text{Mn}_{0.27}]\text{O}_2$ and (B) spoke-like nanorod assemblies (SNAs) $\text{Na}[\text{Ni}_{0.61}\text{Co}_{0.12}\text{Mn}_{0.27}]\text{O}_2$ particles. (C) Schematic diagram for single-particle microcompression tests and (D) corresponding results of $\text{Na}[\text{Ni}_{0.61}\text{Co}_{0.12}\text{Mn}_{0.27}]\text{O}_2$ and $\text{Na}[\text{Ni}_{0.61}\text{Co}_{0.12}\text{Mn}_{0.27}]\text{O}_2$. Reproduced with permission: Copyright 2016, Wiley¹⁶¹

electrolyte. Ti-doped $\text{Na}[\text{Ti}_{0.03}(\text{Ni}_{0.6}\text{Co}_{0.2}\text{Mn}_{0.2})_{0.97}]\text{O}_2$ shows obvious improvement in capacity, cycle stability, rate performance, and thermodynamic performance. The full cell composed of O3- $\text{Na}[\text{Ti}_{0.03}(\text{Ni}_{0.6}\text{Co}_{0.2}\text{Mn}_{0.2})_{0.97}]\text{O}_2$ and hard carbon delivers an excellent cycle retention of 77% over 400 cycles. Yang et al. successfully synthesized P2- $\text{Na}_{0.560}[\text{Li}_{0.041}\text{Mn}_{0.642}\text{Ni}_{0.221}\text{Ti}_{0.095}]\text{O}_2$ via a chemical-precipitation-assisted solid-state reaction.¹⁶⁶ The codoping of Li and Ti contributes to the stable release of lattice stress and the stabilization of the lattice. After 100 cycles between 2.5 and 4.5 V, it shows high capacity retention of 74.2% and high-voltage retention of 95.9%. Besides, the performance of P2-type $\text{Na}_{0.67}\text{Ni}_{0.22}\text{Cu}_{0.11}\text{Mn}_{0.56}\text{Ti}_{0.11}\text{O}_2$ under water-processing conditions was investigated.¹⁶⁷ It achieves an initial discharge capacity of 180 mAh g^{-1} with an energy density of 544 Wh kg^{-1} at 22°C . The aging

tests demonstrate that it has excellent water resistance stability and is almost unaffected by volume structure or chemical changes. The water-processed $\text{Na}_{0.67}\text{Ni}_{0.22}\text{Cu}_{0.11}\text{Mn}_{0.56}\text{Ti}_{0.11}\text{O}_2$ delivers stable cycling performance with minor voltage decay.

As a cost-effective element, Mg is widely used in the electrochemical modification of materials. Mg-substituted $\text{Na}_{0.67}\text{Mn}_{0.65}\text{Ni}_{0.2}\text{Co}_{0.15-x}\text{Mg}_x\text{O}_2$ compounds were investigated by Wen et al.¹⁶⁴ In situ XRD results show that $\text{Na}_{0.67}\text{Mn}_{0.65}\text{Ni}_{0.2}\text{Co}_{0.15}\text{O}_2$ can maintain the P2 structure even when charged to 4.3 V, which is due to the alleviation of lattice parameters and cell volume changes, as shown in Figure 12B. After the introduction of magnesium, obvious improvement in electrochemical performance and less CO_2 evolution were observed. P2-type $\text{Na}_{0.5}\text{Mn}_{0.6}\text{Ni}_{0.2}\text{Cu}_{0.1}\text{Mg}_{0.1}\text{O}_2$ has also been proven to be a

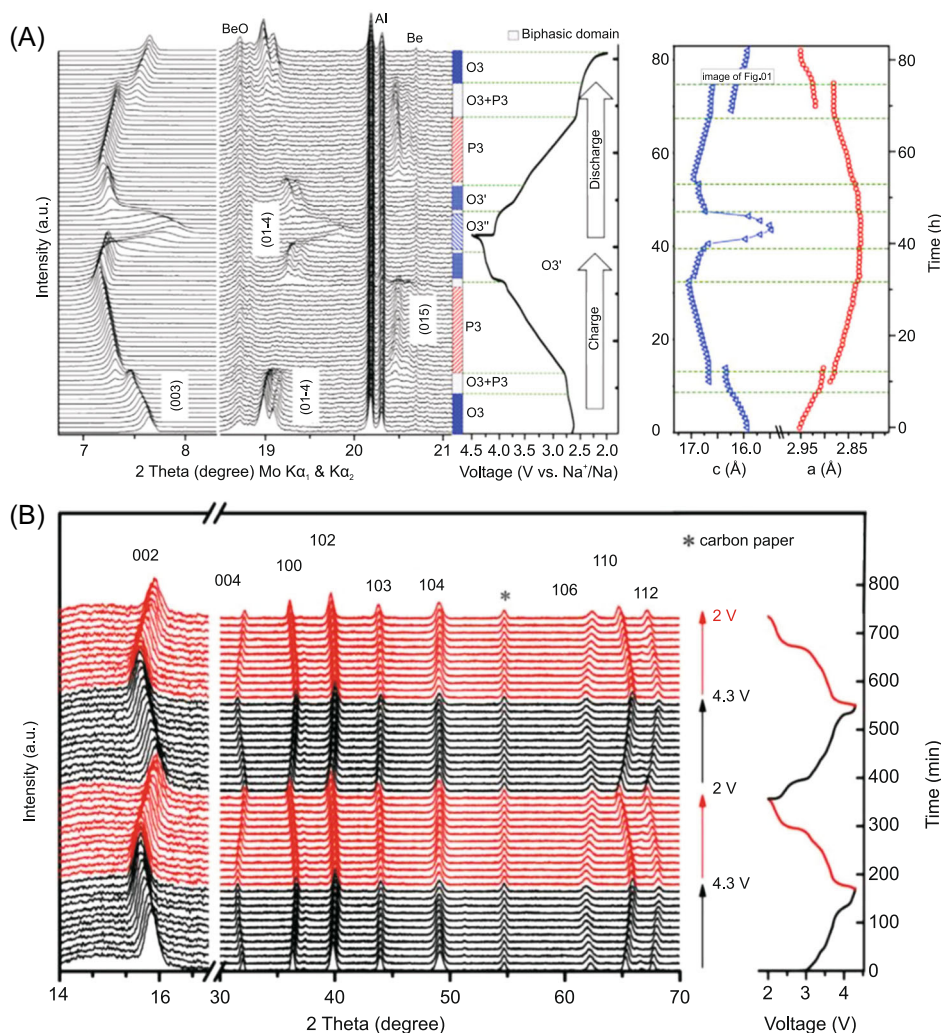


FIGURE 12 (A) In situ XRD patterns of the O3- $\text{Na}(\text{Mn}_{0.25}\text{Fe}_{0.25}\text{Co}_{0.25}\text{Ni}_{0.25})\text{O}_2$ cathode (left), corresponding to the galvanostatic charge and discharge curves (middle), and the lattice parameter evolution (right). Reproduced with permission: Copyright 2014, Elsevier.¹⁶² (B) In situ X-ray diffraction patterns of P2- $\text{Na}_{0.67}\text{Mn}_{0.65}\text{Ni}_{0.2}\text{Co}_{0.15}\text{O}_2$ and corresponding charge and discharge profiles. Reproduced with permission: Copyright 2019, Elsevier¹⁶⁴

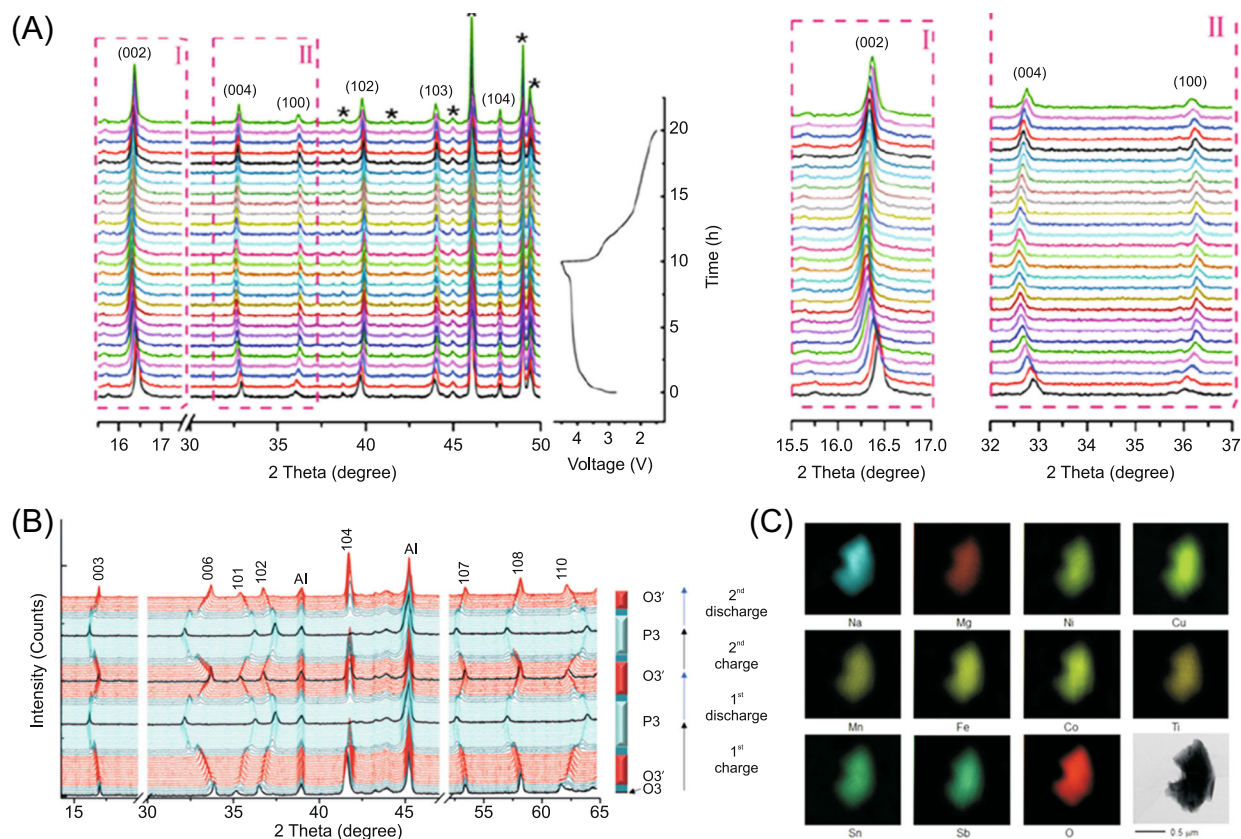


FIGURE 13 (A) In situ X-ray diffraction (XRD) patterns of $\text{Na}_{0.66}\text{Li}_{0.18}\text{Mn}_{0.71}\text{Mg}_{0.21}\text{Co}_{0.08}\text{O}_2$ collected during the initial charge/discharge process. Reproduced with permission: Copyright 2019, American Chemical Society.¹⁶⁹ (B) In situ XRD patterns of $\text{NaNi}_{0.12}\text{Cu}_{0.12}\text{Mg}_{0.12}\text{Fe}_{0.15}\text{Co}_{0.15}\text{Mn}_{0.1}\text{Ti}_{0.1}\text{Sn}_{0.1}\text{Sb}_{0.04}\text{O}_2$ collected at 0.1 C in the voltage range of 2.0–3.9 V, and (C) transmission electron microscope (HRTEM) image and energy dispersive X-ray spectroscopy (EDS) mappings for elements. Reproduced with permission: Copyright 2020, Wiley¹⁷¹

promising cathode with excellent stability, high operation voltage, and high energy density for SIBs.¹⁶⁸ Cu and Mg cosubstitution suppresses the P2–O2 phase transition and extends cell parameters to facilitate Na^+ deintercalation and intercalation. The P2- $\text{Na}_{0.5}\text{Mn}_{0.6}\text{Ni}_{0.2}\text{Cu}_{0.1}\text{Mg}_{0.1}\text{O}_2$ cathode shows a reversible specific capacity of 126.1 mAh g^{-1} at 0.1 C with 96.7% capacity retention after 100 cycles and 3.6 V high average discharge voltage. In addition, the full cell matched with the hard carbon anode delivers a reversible specific capacity of 70.8 mAh g^{-1} with a high energy density of up to $226.56 \text{ Wh kg}^{-1}$. Even after 200 cycles at 0.5 C, the full cell shows an excellent capacity retention of 90.1%, indicating the possibility of its use in practical applications.

Replacement of transition-metal sites with electrochemically inactive Li allows the construction of stable structures. P2 and O3 composite layered $\text{Na}_{0.95}\text{Li}_{0.15}\text{Ni}_{0.15}\text{Mn}_{0.55}\text{Co}_{0.1}\text{O}_2$ was proposed to be a competitive cathode for SIBs.¹⁶⁹ The novel P2 + O3 $\text{Na}_{0.95}\text{Li}_{0.15}\text{Ni}_{0.15}\text{Mn}_{0.55}\text{Co}_{0.1}\text{O}_2$ delivers a large discharge capacity of 200 mAh g^{-1} . In the meantime, it also presents a large

discharge capacity of 134 mAh g^{-1} at 1 C and 75% retention after 150 cycles at 0.5 C. The energy density of this cathode is up to 640 mAh g^{-1} , which is comparable to that of LIBs. Wang and coworkers synthesized a new P2-type $\text{Na}_{0.66}\text{Li}_{0.18}\text{Mn}_{0.71}\text{Mg}_{0.21}\text{Co}_{0.08}\text{O}_2$ cathode with nanosize primary crystalline particles and secondary spheres with uniform microsize via the solvothermal method and a solid-state reaction.¹⁷⁰ It delivers high initial discharge capacity (166 mAh g^{-1}) and superior retention (82% after 100 cycles at 20 mA g^{-1}). The in situ XRD patterns suggest that a stable and highly reversible P2-type structure is maintained during the desodiation/sodiation process (Figure 13A). To overcome the irreversible phase change problem, our group designed and synthesized a P2-type $\text{Na}_{0.8}\text{Li}_{0.1}\text{Mn}_{0.6}\text{Ni}_{0.2}\text{Cu}_{0.1}\text{O}_2$ cathode via the coprecipitation method.⁴⁹ As an inert element, Li is embedded in transition-metal sites, playing the role of a structural supporting site for lattice strain. The electrochemical performance test results show that $\text{Na}_{0.8}\text{Li}_{0.1}\text{Mn}_{0.6}\text{Ni}_{0.2}\text{Cu}_{0.1}\text{O}_2$ delivers an initial discharge capacity of 135.1 mAh g^{-1} at a current of 0.1 C with 83.1% retention

over 100 cycles. Even at 1 A g^{-1} , it still maintains a retention of 81.7% after 400 cycles with 84.7 mAh g^{-1} discharge capacity, indicating excellent rate performance. The results of the GITT show high diffusivity of Na^+ , and XRD results prove that the pure P2 structure is maintained during the charge and discharge process.

DFT calculations demonstrate that cosubstitution of one kind of heteroatom with comparable electronegativity and another one with a different Fermi level can overcome the problems of the spontaneous extraction of Na and oxidation of transition metals in air.⁶⁷ Based on the adjustment of the electronic structure and a combination of transition metals, Wan and his partners modulated $\text{NaNi}_{0.5}\text{Mn}_{0.5}\text{O}_2$ via Cu/Ti codoping. Rietveld refinement, electrochemistry, and XPS tests clearly demonstrate the modulation. The as-prepared O_3 -type $\text{NaNi}_{0.45}\text{Cu}_{0.05}\text{Mn}_{0.4}\text{Ti}_{0.1}\text{O}_2$ presents better air stability than $\text{NaNi}_{0.5}\text{Mn}_{0.5}\text{O}_2$, which possess longer circulation time and higher capacity retention under air exposure. Even after being soaked in water, $\text{NaNi}_{0.45}\text{Cu}_{0.05}\text{Mn}_{0.4}\text{Ti}_{0.1}\text{O}_2$ retains its structure and capacity. The charge ordering and complicated phase transitions are successfully suppressed during cycling. Single-phase P2- $\text{Na}_{0.67}\text{Mn}_{0.6}\text{Ni}_{0.2}\text{Co}_{0.1}\text{Cu}_{0.1}\text{O}_2$ has also been proven to be a promising cathode with excellent electrochemical performance.¹⁷² It comprises of multiple-layer-oriented stacked nanoflakes and presents a large three-dimensional frame, which facilitates the diffusion of sodium ions. The slight volume shrinkage and stable single-phase structure Na^+ extraction ensure the excellent rate performance. Moreover, Cu- $\text{Na}_{0.67}\text{Mn}_{0.6}\text{Ni}_{0.2}\text{Co}_{0.2}\text{O}_2$ with surface doped with Cu excellent stability.¹⁷³ The copper-rich surface layer inhibits side reactions at the electrode/electrolyte interface and reduces the dissolution of manganese during the charge and discharge process.

For transition-metal oxides, the general traditional metal doping method involves replacement of the transition metal with external metal ions to control the structure and morphology of the target material. Unlike widely used doping methods, Liu et al. introduced a high-valence metal (Sr^{2+}) into sodium ion layers to modify layered oxides, which provides a new strategy for the modification of cathodes.¹⁷⁴ P2- $\text{Na}_{0.57}\text{Sr}_{0.05}\text{Mn}_{0.6}\text{Ni}_{0.2}\text{Co}_{0.2}\text{O}_2$ was constructed using a sol-gel method, and it consisted of multiple-layer oriented stacking nanoflakes. Owing to the substitution of Sr^{2+} for Na^+ ions, equivalent Na^+ /vacancies are formed. Large-radius Sr^{2+} is embedded in the Na ion layers, which increases the layer spacing and provides wide Na-ion transport channels. Under the combined action of the Na^+ /vacancies and wide ionic channels, $\text{Na}_{0.57}\text{Sr}_{0.05}\text{Mn}_{0.6}\text{Ni}_{0.2}\text{Co}_{0.2}\text{O}_2$ presents excellent ionic diffusion ability and low transport energy barrier (0.79 eV). It delivers an initial specific capacity of 120.9 mAh g^{-1} with 85.6% retention after 200 cycles.

As a new approach, high-entropy oxides, which consist of five or more major elements sharing the equiatomic sites, are used to develop advanced cathodes with unique properties. For example, a layered O_3 - $\text{NaNi}_{0.12}\text{Cu}_{0.12}\text{Mg}_{0.12}\text{Fe}_{0.15}\text{Co}_{0.15}\text{Mn}_{0.1}\text{Ti}_{0.1}\text{Sn}_{0.1}\text{Sb}_{0.04}\text{O}_2$ has been successfully synthesized.¹⁷¹ It shows long-term cycling stability with superior 83% capacity retention after 500 cycles at 3 C. Highly reversible O_3 -P3 phase transition occurs during the charge and discharge process, which contributes more than 60% of the total capacity, as shown in Figure 13B. Uniformly distributed elements show the successful formation of high-entropy oxides (Figure 13C). Entropy stabilization on the host matrix yields the P2 structure, resulting in excellent cycling stability and rate performance. For air-stable layered cathode, $\text{Na}[\text{Li}_{0.05}\text{Mn}_{0.50}\text{Ni}_{0.30}\text{Cu}_{0.10}\text{Mg}_{0.05}]\text{O}_2$ is a promising candidate to promote progress toward commercialization of SIBs.¹⁷⁵ It delivers a reversible specific capacity of 172 mAh g^{-1} at a current density of 0.1 C and 70.4% capacity retention after 1000 cycles at 20 C. When assembled with a pristine hard carbon anode, promising application prospects were demonstrated by high energy density up to 215 Wh kg^{-1} at 0.1 C. Besides, Lin and coworkers reported $\text{Na}_{0.75}\text{Co}_{0.125}\text{Cu}_{0.125}\text{Fe}_{0.125}\text{Ni}_{0.125}\text{Mn}_{0.5}\text{O}_2$ with intergrowth of ordered P2 and P3 phases.¹⁷⁶ It can achieve 100% capacity retention at 0.1 C after 100 cycles and 85% capacity retention at 5 C after 1000 cycles. Furthermore, other multivalent layered oxides have also been extensively studied.¹⁷⁷⁻¹⁷⁹

5 | SUMMARY AND PERSPECTIVES

In recent years, remarkable achievements have been made in the research of metal oxide cathode materials for SIBs. In this review, we have comprehensively summarized progress in the research of oxide cathode electrodes, as shown in Table 1. Moreover, the current key issues and cutting-edge solutions have been proposed. Irreversible phase transition, insufficient specific reversible capacity, instability of material surface, and the high cost of Co/Ni-layered oxides are the main obstacles at present. To overcome these issues, we propose a series of strategies to obtain advantageous oxide cathode materials, including cation doping in the crystal framework, inducing anion redox reactions, coating a protective layer on the surface, exploring Co/Ni-free materials, and so forth. Among all the modification strategies, cation doping is generally considered to be the most effective one, which provides a conspicuous improvement in electrochemical performance. For future research work, an in-depth investigation of the charge compensation and phase transformation mechanisms should be performed. Furthermore, the current performance

TABLE 1 Summary of current mental oxide cathodes on phase transition and electrochemical performance

Materials	Phase	Voltage range (V)	Reversible capacity (mAh g ⁻¹)	Capacity retention	References
NaMnO ₂	O3	2.0–3.8	185/0.1 C	80.5%/10 cycles	[72]
Na _{0.67} MnO ₂	P2	1.5–4.3	205/0.1 C	83.3%/30 cycles	[180]
Na _{0.6} MnO ₂	P2	2.0–3.8	140/0.1 C	85%/4 cycles	[181]
Na ₄ Mn ₉ O ₁₈	Tunnel	2.0–4.0	110/0.5 C	77%/1000 cycles	[33]
Na _{0.7} CoO ₂	P2	2.0–3.8	114/0.4 C	86%/300 cycles	[182]
NaNiO ₂	O3	1.25–3.75	123/0.1 C	94.3%/20 cycles	[94]
C-NaCrO ₂	O3	2.0–3.6	112/20 mA g ⁻¹	90%/300 cycles	[29]
NaFeO ₂	O3	2.5–3.4	80/12 mA g ⁻¹	75%/30 cycles	[88]
Na _{0.7} VO ₂	P2	1.2–2.4	100/0.05 C	Unknown	[105]
Na _{0.78} Ni _{0.23} Mn _{0.69} O ₂	P2	2.0–4.5	138/0.1 C	87.6%/20 cycles	[183]
Na _{2/3} [Mg _{0.28} Mn _{0.72}]O ₂	P2	1.5–4.4	220/20 mA g ⁻¹	68.1%/30 cycles	[128]
Na _{0.72} [Li _{0.24} Mn _{0.76}]O ₂	P2	1.5–4.5	270/0.05 C	54.8%/30 cycles	[64]
Na _{0.6} Mn _{0.8} Li _{0.2} O ₂	P2	2.0–4.6	190/(C/20)	100%/100 cycles	[122]
NaNi _{0.5} Mn _{0.5} O ₂	O3	2.0–4.0	141/0.05 C	90%/100 cycles	[184]
Na ₃ Ni ₂ SbO ₆	O'3	2.0–4.0	117/20 mA g ⁻¹	95%/50 cycles	[134]
Na _{2/3} Fe _{1/2} Mn _{1/2} O ₂	P2	1.5–4.3	190/0.05 C	81.5%/30 cycles	[114]
Na ₃ Ni ₂ BiO ₆	O'3	2.0–4.0	106/0.05 C	91%/50 cycles	[133]
Na _{0.8} Ni _{0.4} Ti _{0.6} O ₂	O3	2.0–4.0	83/0.2 C	Unknown	[185]
Na _{5/6} [Li _{1/4} Mn _{3/4}]O ₂	P2	1.5–4.4	200/20 mA g ⁻¹	Unknown	[186]
NaNi _{0.5} Ti _{0.5} O ₂	O2	2.0–4.7	121/20 mA g ⁻¹	52.8%/50 cycles	[137]
Na _{2/3} Fe _{2/3} Mn _{1/3} O ₂	P2	1.5–4.2	151/24 mA g ⁻¹	81.3%/10 cycles	[187]
NaNi _{0.5} Fe _{0.5} O ₂	O3	2.0–3.9	129/23.8 mA g ⁻¹	94%/20 cycles	[139]
NaFe _{0.5} Co _{0.5} O ₂	O3	2.5–4.0	160/12 mA g ⁻¹	84%/50 cycles	[188]
Na _{0.6} Ti _{0.48} Mn _{0.52} O ₂	Tunnel	1.5–4.0	86/0.2 C	81.39%/100 cycles	[189]
Na _{0.44} Mn _{0.89} Ti _{0.11} O ₂	Tunnel	2.0–4.0	96/5 C	74%/1000 cycles	[190]
Na _{0.67} Co _{0.5} Mn _{0.5} O ₂	P2	1.5–4.3	147/0.1 C	100%/100 cycles	[112]
Na ₂ RuO ₃	O3	1.5–4.0	180/30 mA g ⁻¹	88.8/50 cycles	[37]

(Continues)

TABLE 1 (Continued)

Materials	Phase	Voltage range (V)	Reversible capacity (mAh g ⁻¹)	Capacity retention	References
Na _{0.66} Li _{0.22} Ru _{0.78} O ₂	P2	1.5–4.5	150/50 mA g ⁻¹	91%/500 cycles	[127]
Na ₂ Ru _{0.9} Mn _{0.1} O ₃	O3	1.5–4.5	142.76/100 mA g ⁻¹	75.72%/100 cycles	[191]
Na _{2/3} Mn _{0.95} Mg _{0.05} O ₂	P2	1.5–4.0	146/1 A g ⁻¹	95.9%/50 cycles	[192]
NaCo _{0.7} Mn _{0.3} O ₂	P2	2.0–4.1	95/1 C	84%/225 cycles	[113]
Na _{2/3} Fe _{0.4} Mn _{0.6} O ₂	P2	1.5–4.2	146/15 mA g ⁻¹	65%/20 cycles	[193]
Na _{0.67} Mn _{0.7} Ni _{0.2} Mg _{0.1} O ₂	P2	2.0–4.5	128/12 mA g ⁻¹	95.4%/50 cycles	[194]
Na _{0.67} Mn _{0.8} Ni _{0.1} Mg _{0.1} O ₂	P2	1.5–4.2	123/0.1 C	85%/50 cycles	[195]
Na _{0.67} Ni _{0.23} Mg _{0.1} Mn _{0.67} O ₂	P2	2.0–4.5	105/48 mA g ⁻¹	80.85%/100 cycles	[196]
Na _{0.67} Mn _{0.7} Ni _{0.1} Cu _{0.2} O ₂	P2	2.0–4.5	115/0.1 C	90%/50 cycles	[53]
Na _{0.44} Mn _{0.6} Ni _{0.3} Cu _{0.1} O ₂	P2	1.5–4.0	149/0.1 C	80%/50 cycles	[140]
Na _{2/3} Mn _{2/3} Ni _{1/4} Cu _{1/12} O ₂	P2	2.5–4.4	130/12 mA g ⁻¹	75%/30 cycles	[152]
Na _{0.70} Mn _{0.60} Ni _{0.30} Co _{0.10} O ₂	P2	1.7–4.0	125/10 mA g ⁻¹	91%/20 cycles	[197]
NaNi _{0.6} Co _{0.05} Mn _{0.35} O ₂	O3	1.5–3.9	157/15 mA g ⁻¹	84%/100 cycles	[160]
Na[Ni _{0.61} Co _{0.12} Mn _{0.27}]O ₂	O3	1.5–4.1	153/0.5 C	80%/100 cycles	[161]
Na _{0.67} [Mn _{0.65} Co _{0.2} Ni _{0.15}]O ₂	P2	2.0–4.4	141/0.1 C	88.6%/50 cycles	[176]
Na _{0.67} [Mn _{0.65} Ni _{0.15} Co _{0.15} Al _{0.05}]O ₂	P2	2.0–4.4	129/0.1 C	95.3%/50 cycles	[176]
Na _x Ni _{1/3} Mn _{1/3} Co _{1/3} O ₂	P2	2.0–4.4	142.8/0.1 C	93.13%/50 cycles	[198]
NaNi _{1/3} Mn _{1/3} Co _{1/3} O ₂	O3	2.0–3.75	120/0.1 C	Unknown	[149]
Na _{2/3} Co _{2/3} Mn _{2/9} Ni _{1/9} O ₂	P2	2.0–4.2	80/0.05 C	89%/90 cycles	[199]
Na _{0.66} (Mn _{0.54} Co _{0.13} Ni _{0.13})O ₂	P2	2.0–4.5	121/1 C	50%/100 cycles	[200]
Na _{0.65} [Ni _{0.17} Co _{0.11} Mn _{0.72}]O ₂	P2	1.5–4.3	187/12 mA g ⁻¹	74.7%/500 cycles	[201]
Na _{0.7} Mn _{0.7} Ni _{0.2} Co _{0.1} O ₂	P2	1.5–4.2	148/0.1 C	95%/50 cycles	[151]
Na _{2/3} Ni _{1/3} Mn _{5/9} Al _{1/9} O ₂	P2	1.6–4.0	118/0.1 C	77.5%/100 cycles	[146]
Na _{0.8} Li _{0.12} Ni _{0.22} Mn _{0.66} O ₂	P2	2.0–4.4	133/12 mA g ⁻¹	86%/50 cycles	[202]
Na _{0.7} Li _{0.3} Ni _{0.5} Mn _{0.5} O ₂ + d	P2/O3	2.0–4.05	125/15 mA g ⁻¹	95%/20 cycles	[203]
Na[Ni _{1/3} Fe _{1/3} Mn _{1/3}]O ₂	O3	1.5–4.1	100/0.5 C	Unknown	[204]
Na _{2/3} Ni _{1/3} Mn _{1/2} Ti _{1/6} O ₂	P2	2.5–4.35	127/12 mA g ⁻¹	94%/10 cycles	[205]

TABLE 1 (Continued)

Materials	Phase	Voltage range (V)	Reversible capacity (mAh g ⁻¹)	Capacity retention	References
Na _{0.66} Mn _{0.67} Ni _{0.26} Zn _{0.07} O ₂	P2	2.2–4.25	132/12 mA g ⁻¹	89%/30 cycles	[145]
Na _{2/3} Ni _{1/3} Mn _{1/3} Ti _{1/3} O ₂	P2	2.5–4.15	88/1 C	83.9%/500 cycles	[206]
NaNi _{0.5} Mn _{0.2} Ti _{0.3} O ₂	O3	2.0–4.0	130/1 C	85%/200 cycles	[143]
Na _{0.7} Mg _{0.05} [Mn _{0.6} Ni _{0.2} Mg _{0.15}]O ₂	P2	1.5–4.2	75/1 C	79%/1000 cycles	[154]
Na _{7/9} Cu _{2/9} Fe _{1/9} Mn _{2/3} O ₂	P2	2.5–4.2	89/10 mA g ⁻¹	87%/150 cycles	[207]
Na _{0.9} Cu _{0.22} Fe _{0.30} Mn _{0.48} O ₂	O3	2.5–4.05	100/10 mA g ⁻¹	97%/100 cycles	[55]
Na _{2/3} Ni _{1/6} Co _{1/6} Ti _{2/3} O ₂	P2	2.0–4.0	55/0.2 C	94.3%/500 cycles	[208]
Na _{2/3} Mn _{0.8} Fe _{0.1} Ti _{0.1} O ₂	P2	2.0–4.0	144/24.5 mA g ⁻¹	95.09%/50 cycles	[118]
Na _{2/3} Fe _{2/9} Ni _{2/9} Mn _{5/9} O ₂	P2	2.5–4.3	130/0.5 C	78%/100 cycles	[62]
Na _{0.7} Bi _{0.01} MnO ₂	P2/tunnel/O3'	2.0–4.1	86.2/0.5 C	86.2%/100 cycles	[209]
PL-Na _{2/3} (Mn _{0.54} Ni _{0.13} Co _{0.13})O ₂	P2	2.0–4.5	135/0.16 A g ⁻¹	82%/100 cycles	[157]
NaNi _{1/3} Fe _{1/3} Mn _{1/3} O ₂	O3	2.0–4.0	122/130 mA g ⁻¹	80%/100 cycles	[210]
Na _{2/3} Ni _{1/6} Mn _{2/3} Cu _{1/9} Mg _{1/18} O ₂	P2	2.0–4.5	64/5 C	73%/500 cycles	[211]
Na _{0.66} Li _{0.18} Mn _{0.71} Mg _{0.21} Co _{0.08} O ₂	P2	1.5–4.5	166/0.1 C	82%/100 cycles	[170]
Na _{0.5} Mn _{0.6} Ni _{0.2} Cu _{0.1} Mg _{0.1} O ₂	P2	2.0–4.6	126.1/0.1 C	96.7%/100 cycles	[168]
Na _{0.8} Li _{0.1} Mn _{0.6} Ni _{0.2} Cu _{0.1} O ₂	P2	1.8–4.0	135.1/0.1 C	83.1%/100 cycles	[49]
Na _{0.67} Mn _{0.6} Ni _{0.2} Co _{0.1} Cu _{0.1} O ₂	P2	1.9–4.0	131.3/0.1 C	86.7%/200 cycles	[172]
NaNi _{0.4} Mn _{0.4} Cu _{0.1} Ti _{0.1} O ₂	O3	2.0–4.0	116/0.2 C	84%/100 cycles	[212]
Na _{0.57} St _{0.05} Mn _{0.64} Ni _{0.2} Co _{0.2} O ₂	P2	1.9–4.0	120.9/0.1 C	85.6%/200 cycles	[174]
Na _{0.56} [Li _{0.041} Mn _{0.642} Ni _{0.221} Ti _{0.095}]O ₂	P2	2.5–4.5	137.7/0.1 C	74.2%/100 cycles	[166]
Na _{0.67} Ni _{0.22} Cu _{0.11} Mn _{0.56} Ti _{0.11} O ₂	P2	2.5–4.5	115/0.2 C	84%/50 cycles	[167]
Na[Li _{0.03} (Ni _{0.6} Co _{0.2} Mn _{0.2}) _{0.97}]O ₂	O3	1.5–4.1	151/0.1 C	93%/100 cycles	[165]
Na _{0.85} Li _{0.12} Ni _{0.22} Mn _{0.66} O ₂	P2	2–4.3	104.8/5 C	85.4%/500 cycles	[213]
Na _{0.8} [Ni _{1/5} Fe _{1/5} Co _{1/5} Mn _{1/5} Ti _{1/5}]O ₂	O3	2.0–4.0	107/0.05 C	90%/100 cycles	[177]
NaNi _{0.12} Cu _{0.12} Mg _{0.12} Fe _{0.15} Co _{0.15} Mn _{0.1} Ti _{0.1} Sb _{0.04} O ₂	O3	2.0–3.9	90/3.0 C	83%/500 cycles	[171]
Na[Li _{0.05} (Ni _{0.25} Fe _{0.25} Mn _{0.5}) _{0.95}]O ₂	O3	1.75–4.4	180/0.1 C	92.1%/40 cycles	[214]
NaNi _{1/4} Co _{1/4} Fe _{1/4} Ti _{1/4} O ₂	O3	2.0–3.9	116/12 mA g ⁻¹	75%/400 cycles	[215]

(Continues)

TABLE 1 (Continued)

Materials	Phase	Voltage range (V)	Reversible capacity (mAh g ⁻¹)	Capacity retention	References
NaMn _{0.25} Fe _{0.25} Co _{0.25} Ni _{0.25} O ₂	O3	1.9–4.3	180/0.1 C	85%/20 cycles	[162]
Na ₃ Ni _{1.7} Mg _{0.3} SbO ₆	O3	2.0–3.8	120/0.1 C	78%/200 cycles	[216]
Na[Li _{0.05} Mn _{0.50} Ni _{0.30} Cu _{0.10} Mg _{0.05}]O ₂	O3	2.0–4.0	172/0.1 C	87.7%/200 cycles	[175]
Na _{0.86} Co _{0.475} Mn _{0.475} Ti _{0.05} O ₂	P2	1.5–4.0	98.8/1 C	81.9/100 cycles	[217]
Na _{0.66} Li _{0.18} Mn _{0.71} Ni _{0.21} Co _{0.08} O _{2+d}	P2/O3	1.5–4.5	200/10 mA g ⁻¹	75%/150 cycles	[169]

evaluation of electrode materials is mainly carried out in the half-cell system with metallic sodium as the counter electrode. It is difficult to use Na metal as the anode material in practical applications due to its potential safety risks and dendrite problem. As is well known, the electrochemical performance of half-cells is different from that of full-cells. The research of a full-cell system is crucial, as it plays a role in bridging half-cells and practical application for SIBs. To design a full-cell system with high energy density, long cycle life, good safety, and competitive cost, stable anodes, cathodes, and electrolytes should be rationally selected. Although limited research has been carried out to assemble the full cell for exploration, it is not enough for the application of SIBs. Some major challenges remain to be overcome at present, but the rapid progress in this area, coupled with the continued attention of industry and academia, ensures that the future of SIBs does look promising indeed.

ACKNOWLEDGMENTS

This study was supported by the National Natural Science Foundation of China (No. 21471162) and the Hunan Provincial Innovation Foundation for Post graduate (No. 502211822).

CONFLICT OF INTEREST

The authors declare no conflict of interest.

ORCID

Kaiyu Liu  <http://orcid.org/0000-0002-8104-2223>

REFERENCES

- Sun YK, Chen Z, Noh HJ, et al. Nanostructured high-energy cathode materials for advanced lithium batteries. *Nat Mater*. 2012;11(11):942-947.
- Armand M, Tarascon JM. Building better batteries. *Nature*. 2008;451(7179):652-657.
- Yin YX, Xin S, Guo YG, Wan LJ. Lithium-sulfur batteries: electrochemistry, materials, and prospects. *Angew Chem Int Ed*. 2013;52(50):13186-13200.
- Cheng F, Liang J, Tao Z, Chen J. Functional materials for rechargeable batteries. *Adv Mater*. 2011;23(15):1695-1715.
- Gong Z, Yong Y. Recent advances in the research of polyanion-type cathode materials for Li-ion batteries. *Energy Environ Sci*. 2011;4(9):3223-3242.
- Hong SY, Kim Y, Park Y, Choi A, Choi NS, Lee KT. Charge carriers in rechargeable batteries: Na ions vs. Li ions. *Energy Environ Sci*. 2013;6(7):2067-2081.
- Wang Y, Chen R, Chen T, et al. Emerging non-lithium ion batteries. *Energy Stor Mater*. 2016;4:103-129.
- Palomares V, Serras P, Villaluenga I, Hueso KB, Carretero-González J, Rojo T. Na-ion batteries, recent advances and present challenges to become low cost energy storage systems. *Energy Environ Sci*. 2012;5(3):5884-5901.

9. Chen S, Wu C, Shen L, et al. Challenges and perspectives for NASICON-type electrode materials for advanced sodium-ion batteries. *Adv Mater.* 2017;29(48):1700431.
10. Kim SW, Seo DH, Ma X, Ceder G, Kang K. Electrode materials for rechargeable sodium-ion batteries: potential alternatives to current lithium-ion batteries. *Adv Energy Mater.* 2012;2(7):710-721.
11. Pan H, Hu YS, Chen L. Room-temperature stationary sodium-ion batteries for large-scale electric energy storage. *Energy Environ Sci.* 2013;6(8):2338.
12. Guo S, Yi J, Zhou H. Recent advances in titanium-based electrode materials for stationary sodium-ion batteries. *Energy Environ Sci.* 2016;9(10):2978-3006.
13. Fang C, Huang Y, Zhang W, et al. Routes to high energy cathodes of sodium-ion batteries. *Adv Energy Mater.* 2016;6(5):1501727.
14. Wang PF, You Y, Yin YX, Guo YG. Layered oxide cathodes for sodium-ion batteries: phase transition, air stability, and performance. *Adv Energy Mater.* 2018;8(8):1701912.
15. Yabuuchi N, Kubota K, Dahbi M, Komaba S. Research development on sodium-ion batteries. *Chem Rev.* 2014;114(23):11636-11682.
16. Liu Z, Yu XY, Lou XW, Paik U. Sb@C coaxial nanotubes as a superior long-life and high-rate anode for sodium ion batteries. *Energy Environ Sci.* 2016;9(7):2314-2318.
17. Hwang JY, Myung ST, Sun YK. Sodium-ion batteries: present and future. *Chem Soc Rev.* 2017;46(12):3529-3614.
18. Man HH, Gonzalo E, Singh G, Rojo T. A comprehensive review of sodium layered oxides: powerful cathodes for Na-ion batteries. *Energy Environ Sci.* 2015;8(1):81-102.
19. Wang S, Sun C, Wang N, Zhang Q. Ni- and/or Mn-based layered transition metal oxides as cathode materials for sodium ion batteries: status, challenges and countermeasurements. *J Mater Chem A.* 2019;7(17):10138-10158.
20. Qi Y, Tong Z, Zhao J, et al. Scalable room-temperature synthesis of multi-shelled Na₃(VOPO₄)₂F microsphere cathodes. *Joule.* 2018;2(11):2348-2363.
21. Qian J, Wu C, Cao Y, et al. Prussian blue cathode materials for sodium-ion batteries and other ion batteries. *Adv Energy Mater.* 2018;8(17):1702619.
22. Luo W, Allen M, Raju V, Ji X. An organic pigment as a high-performance cathode for sodium-ion batteries. *Adv Energy Mater.* 2014;4(15):1400554.
23. Li WJ, Chou SL, Wang JZ, et al. Multifunctional conducting polymer coated Na_{1+x}MnFe(CN)₆ cathode for sodium-ion batteries with superior performance via a facile and one-step chemistry approach. *Nano Energy.* 2015;13:200-207.
24. Masquelier C, Croguennec L. Polyanionic (phosphates, silicates, sulfates) frameworks as electrode materials for rechargeable Li (or Na) batteries. *Chem Rev.* 2013;113(8):6552-6591.
25. Ortiz-Vitoriano N, Drewett NE, Gonzalo E, Rojo T. High performance manganese-based layered oxide cathodes: overcoming the challenges of sodium ion batteries. *Energy Environ Sci.* 2017;10(5):1051-1074.
26. Liu T, Zhang Y, Jiang Z, et al. Exploring competitive features of stationary sodium ion batteries for electrochemical energy storage. *Energy Environ Sci.* 2019;12(5):1512-1533.
27. Sun Y, Guo S, Zhou H. Adverse effects of interlayer-gliding in layered transition-metal oxides on electrochemical sodium-ion storage. *Energy Environ Sci.* 2019;12(3):825-840.
28. Zhang K, Kim D, Hu Z, et al. Manganese based layered oxides with modulated electronic and thermodynamic properties for sodium ion batteries. *Nat Commun.* 2019;10:5203.
29. Yu CY, Park JS, Jung HG, et al. NaCrO₂ cathode for high-rate sodium-ion batteries. *Energy Environ Sci.* 2015;8(7):2019-2026.
30. Zhao J, Zhao L, Dimov N, Okada S, Nishida T. Electrochemical and thermal properties of α-NaFeO₂ cathode for Na-ion batteries. *J Electrochem Soc.* 2013;160(5):A3077-A3081.
31. Delmas C, Fouassier C, Hagenmuller P. Structural classification and properties of the layered oxides. *Physica.* 1980;99(1-4):81-85.
32. Stoyanova R, Carlier D, Sendova-Vassileva M, et al. Stabilization of over-stoichiometric Mn⁴⁺ in layered Na_{2/3}MnO₂. *J Solid State Chem.* 2010;183(6):1372-1379.
33. Cao Y, Xiao L, Wang W, et al. Reversible sodium ion insertion in single crystalline manganese oxide nanowires with long cycle life. *Adv Mater.* 2011;23(28):3155-3160.
34. Robertson AD, Bruce PG. Mechanism of electrochemical activity in Li₂MnO₃. *Chem Mater.* 2003;15(10):1984-1992.
35. Koga H, Croguennec L, Ménétrier M, et al. Operando X-ray absorption study of the redox processes involved upon cycling of the Li-rich layered oxide Li_{1.20}Mn_{0.54}Co_{0.13}Ni_{0.13}O₂ in Li ion batteries. *J Phys Chem C.* 2014;118(11):5700-5709.
36. Qiao Y, Guo S, Zhu K, et al. Reversible anionic redox activity in Na₃RuO₄ cathodes: a prototype Na-rich layered oxide. *Energy Environ Sci.* 2018;11(2):299-305.
37. Mortemard de Boisse B, Liu G, Ma J, et al. Intermediate honeycomb ordering to trigger oxygen redox chemistry in layered battery electrode. *Nat Commun.* 2016;7:11397.
38. Yahia, MBen, Vergnet, et al. ML. Unified picture of anionic redox in Li/Na-ion batteries. *Nat Mater.* 2019;18(5):496-502.
39. Hong J, Gent WE, Xiao P, et al. Metal-oxygen decoordination stabilizes anion redox in Li-rich oxides. *Nat Mater.* 2019;18(3):256-265.
40. Zheng W, Liu Q, Wang Z, et al. Oxygen redox activity with small voltage hysteresis in Na_{0.67}Cu_{0.28}Mn_{0.72}O₂ for sodium-ion batteries. *Energy Stor Mater.* 2020;28:300-306.
41. Li XL, Wang T, Yuan Y, et al. Whole-voltage-range oxygen redox in P2-layered cathode materials for sodium-ion batteries. *Adv Mater.* 2021;33(13):2008194.
42. Mortemard de Boisse B, Nishimura S, Watanabe E, et al. Highly reversible oxygen-redox chemistry at 4.1 V in Na_{4/7-x}[□_{1/7}Mn_{6/7}]O₂ (□: Mn vacancy). *Adv Energy Mater.* 2018;8(20):1800409.
43. Zhao C, Wang Q, Lu Y, et al. Decreasing transition metal triggered oxygen redox activity in Na-deficient oxides. *Energy Stor Mater.* 2019;20:395-400.
44. Tournadre F, Croguennec L, Willmann P, Delmas C. On the mechanism of the P2-Na_{0.70}CoO₂ → O₂-LiCoO₂ exchange reaction—part II: an in situ X-ray diffraction study. *J Solid State Chem.* 2004;177(8):2803-2809.
45. Komaba S, Yabuuchi N, Nakayama T, Ogata A, Ishikawa T, Nakai I. Study on the reversible electrode reaction of Na_{1-x}Ni_{0.5}Mn_{0.5}O₂ for a rechargeable sodium-ion battery. *Inorg Chem.* 2012;51(11):6211-6220.

46. Li X, Wang Y, Wu D, Liu L, Bo SH, Ceder G. Jahn–Teller assisted Na diffusion for high performance Na ion batteries. *Chem Mater*. 2016;28(18):6575–6583.
47. Lee DH, Xu J, Meng YS. An advanced cathode for Na-ion batteries with high rate and excellent structural stability. *Phys Chem Chem Phys*. 2013;15(9):3304–3312.
48. Zhang C, Li L, Wang Y, Feng L. Electrochemical properties of P2-Na_{2/3}[Ni_{1/3}Mn_{2/3}]O₂ cathode material for sodium ion batteries when cycled in different voltage ranges. *Electrochim Acta*. 2013;113:200–204.
49. Chen T, Guo J, Zhuo Y, et al. A inactive metal supported oxide cathode material with high rate capability for sodium ion batteries. *Energy Stor Mater*. 2019;20:263–268.
50. Hemalatha K, Jayakumar M, Bera P, Prakash AS. Improved electrochemical performance of Na_{0.67}MnO₂ through Ni and Mg substitution. *J Mater Chem A*. 2015;3(42):20908–20912.
51. Yuan D, Hu X, Qian J, et al. P2-type Na_{0.67}Mn_{0.65}Fe_{0.2}Ni_{0.15}O₂ cathode material with high-capacity for sodium-ion battery. *Electrochim Acta*. 2014;116:300–305.
52. Hwang JY, Myung ST, Aurbach D, Sun YK. Effect of nickel and iron on structural and electrochemical properties of O3 type layer cathode materials for sodium-ion batteries. *J Power Sources*. 2016;324:106–112.
53. Wang L, Sun YG, Hu LL, et al. Copper-substituted Na_{0.67}Ni_{0.3-x}Cu_xMn_{0.7}O₂ cathode materials for sodium-ion batteries with suppressed P2–O2 phase transition. *J Mater Chem A*. 2017;5(18):8752–8761.
54. Talaie E, Duffort V, Smith HL, Fultz B, Nazar LF. Structure of the high voltage phase of layered P2-Na_{2/3-z}[Mn_{1/2}Fe_{1/2}]O₂ and the positive effect of Ni substitution on its stability. *Energy Environ Sci*. 2015;8(8):2512–2523.
55. Mu L, Xu S, Li Y, et al. Prototype sodium-ion batteries using an air-stable and Co/Ni-free O3-layered metal oxide cathod. *Adv Mater*. 2015;27(43):6928–6933.
56. Tamaru M, Wang X, Okubo M, Yamada A. Layered Na₂RuO₃ as a cathode material for Na-ion batteries. *Electrochem Commun*. 2013;33:23–26.
57. Rozier P, Sathiyam M, Paulraj AR, et al. Anionic redox chemistry in Na-rich Na₂Ru_{1-y}Sn_yO₃ positive electrode material for Na-ion batteries. *Electrochem Commun*. 2015;53:29–32.
58. Song S, Kotobuki M, Zheng F, et al. Y-Doped Na₂ZrO₃: a Na-rich layered oxide as a high-capacity cathode material for sodium-ion batteries. *ACS Sustainable Chem Eng*. 2017;5(6):4785–4792.
59. Maitra U, House RA, Somerville JW, et al. Oxygen redox chemistry without excess alkali-metal ions in Na_{2/3}[Mg_{0.28}Mn_{0.72}]O₂. *Nat Chem*. 2018;10:288–295.
60. Rong X, Liu J, Hu E, et al. Structure-induced reversible anionic redox activity in Na layered oxide cathode. *Joule*. 2018;2(1):125–140.
61. Hu E, Yu X, Lin R, et al. Evolution of redox couples in Li- and Mn-rich cathode materials and mitigation of voltage fade by reducing oxygen release. *Nat Energy*. 2018;3(8):690–698.
62. Zhang Y, Wu M, Ma J, et al. Revisiting the Na_{2/3}Ni_{1/3}Mn_{2/3}O₂ cathode: oxygen redox chemistry and oxygen release suppression. *ACS Cent Sci*. 2020;6(2):232–240.
63. Chen T, Fan X, Zhuo Y, Ouyang B, Chen X, Liu K. A monocrystalline orthorhombic Na_{0.44}Mn_{0.9}Li_{0.1}O₂ cathode with outstanding stability and negligible structural strain for sodium-ion batteries. *Inorg Chem Front*. 2021;8(11):2844–2853.
64. Rong X, Hu E, Lu Y, et al. Anionic redox reaction-induced high-capacity and low-strain cathode with suppressed phase transition. *Joule*. 2019;3(2):503–517.
65. Nam KW, Kim S, Yang E, et al. Critical role of crystal water for a layered cathode material in sodium ion batteries. *Chem Mater*. 2015;27(10):3721–3725.
66. Liu Q, Hu Z, Chen M, et al. Recent progress of layered transition metal oxide cathodes for sodium-ion batteries. *Small*. 2019;15(32):e1805381.
67. Yao HR, Wang PF, Gong Y, et al. Designing air-stable O3-type cathode materials by combined structure modulation for Na-ion batteries. *J Am Chem Soc*. 2017;139(25):8440–8443.
68. Kalluri S, Yoon M, Jo M, et al. Feasibility of cathode surface coating technology for high-energy lithium-ion and beyond-lithium-ion batteries. *Adv Mater*. 2017;29(48):1605807.
69. Armstrong AR, Bruce PG. Synthesis of layered LiMnO₂ as an electrode for rechargeable lithium batteries. *Nature*. 1996;381(6582):499–500.
70. Parant JP, Olazcuaga R, Devalette M, Fouassier C, Hagenmuller P. Sur quelques nouvelles phases de formule Na_xMnO₂ (x ≤ 1). *J Solid State Chem*. 1971;3(1):1–11.
71. Mendiboure A, Delmas C, Hagenmuller P. Electrochemical intercalation and deintercalation of Na_xMnO₂ bronzes. *J Solid State Chem*. 1985;58(3):323–331.
72. Ma X, Chen H, Ceder G. Electrochemical properties of monoclinic NaMnO₂. *J Electrochem Soc*. 2011;158(12):A1307–A1312.
73. Billaud J, Clément RJ, Armstrong AR, et al. β-NaMnO₂: a high-performance cathode for sodium-ion batteries. *J Am Chem Soc*. 2014;136(49):17243–17248.
74. Kumakura S, Tahara Y, Kubota K, Chihara K, Komaba S. Sodium and manganese stoichiometry of P2-type Na_{2/3}MnO₂. *Angew Chem Int Ed*. 2016;55(41):12760–12763.
75. He X, Wang J, Qiu B, et al. Durable high-rate capability Na_{0.44}MnO₂ cathode material for sodium-ion batteries. *Nano Energy*. 2016;27:602–610.
76. Ju X, Huang H, Zheng H, et al. A facile method to hunt for durable high-rate capability Na_{0.44}MnO₂. *J Power Sources*. 2018;395:395–402.
77. Hosono E, Saito T, Hoshino J, et al. High power Na-ion rechargeable battery with single-crystalline Na_{0.44}MnO₂ nanowire electrode. *J Power Sources*. 2012;217:43–46.
78. Shinde GS, Nayak PD, Vanam SP, et al. Ultrasonic sonochemical synthesis of Na_{0.44}MnO₂ insertion material for sodium-ion batteries. *J Power Sources*. 2019;416:50–55.
79. Sheng N, Cg H, Lei Y, Zhu C. Controlled synthesis of Na_{0.44}MnO₂ cathode material for sodium ion batteries with superior performance through urea-based solution combustion synthesis. *Electrochim Acta*. 2018;283:1560–1567.
80. Delmas C, Braconnier JJ, Fouassier C, Hagenmuller P. Electrochemical intercalation of sodium in Na_xCoO₂ bronzes. *Solid State Ionics*. 1981;3–4:165–169.
81. Berthelot R, Carlier D, Delmas C. Electrochemical investigation of the P2-Na_xCoO₂ phase diagram. *Nat Mater*. 2011;10(1):74–80.
82. Chou FC, Abel ET, Cho JH, Lee YS. Electrochemical deintercalation, oxygen non-stoichiometry, and crystal growth of Na_xCoO_{2-δ}. *J Phys Chem Solids*. 2005;66(1):155–160.
83. Chou FC, Chu M, Shu GJ, et al. Single crystals by synchrotron X-ray diffraction. *Phys Rev Lett*. 2008;101(12):127404.

84. Lei Y, Li X, Liu L, Ceder G. Synthesis and stoichiometry of different layered sodium cobalt oxides. *Chem Mater.* 2014; 26(18):5288-5296.
85. Takeda Y, Nakahara K, Nishijima M, et al. Sodium deintercalation from sodium iron oxide. *Mater Res Bull.* 1994;29(6): 659-666.
86. Jie Z, Zhao L, Dimov N, Okada S, Nishida T. Electrochemical and thermal properties of α -NaFeO₂ cathode for Na-ion batteries. *J Electrochem Soc.* 2013;160(5):A3077-A3081.
87. Yabuuchi N, Komaba S. Recent research progress on iron- and manganese-based positive electrode materials for rechargeable sodium batteries. *Sci Technol Adv Mater.* 2014; 15(4):043501.
88. Yabuuchi N, Yoshida H, Komaba S. Crystal structures and electrode performance of α -NaFeO₂ for rechargeable sodium batteries. *Electrochemistry.* 2012;80(10):716-719.
89. Li Y, Gao Y, Wang X, et al. Iron migration and oxygen oxidation during sodium extraction from NaFeO₂. *Nano Energy.* 2018;47:519-526.
90. Xu J, Han Z, Jiang K, et al. Suppressing cation migration and reducing particle cracks in a layered Fe-based cathode for advanced sodium-ion batteries. *Small.* 2020;16(3):1904388.
91. Susanto D, Cho MK, Ali G, et al. Anionic redox activity as a key factor in the performance degradation of NaFeO₂ cathodes for sodium ion batteries. *Chem Mater.* 2019;31(10):3644-3651.
92. Silván B, Gonzalo E, Djuandhi L, Sharma N, Fauth F, Saurel D. On the dynamics of transition metal migration and its impact on the performance of layered oxides for sodium-ion batteries: NaFeO₂ as a case study. *J Mater Chem A.* 2018; 6(31):15132-15146.
93. Ohzuku T, Ueda A, Nagayama M. Electrochemistry and structural chemistry of LiNiO₂ (R3m) for 4 volt secondary lithium cells. *J Electrochem Soc.* 1993;140(7):1862-1870.
94. Vassilaras P, Ma X, Li X, Ceder G. Electrochemical properties of monoclinic NaNiO₂. *J Electrochem Soc.* 2012;160(2): A207-A211.
95. Man HH, Gonzalo E, Casas-Cabanas M, Rojo T. Structural evolution and electrochemistry of monoclinic NaNiO₂ upon the first cycling process. *J Power Sources.* 2014;258:266-271.
96. Wang L, Wang J, Zhang X, et al. Unravelling the origin of irreversible capacity loss in NaNiO₂ for high voltage sodium ion batteries. *Nano Energy.* 2017;34:215-223.
97. Braconnier JJ, Delmas C, Hagenmuller P. Etude par desintercalation electrochimique des systemes Na_xCrO₂ et Na_xNiO₂. *Mater Res Bull.* 1982;17(8):993-1000.
98. Myung ST, Komaba S, Hirosaki N, Kumagai N. Preparation of layered LiMn_xCr_{1-x}O₂ solid solution by emulsion drying method as lithium intercalation compounds. *Electrochem Commun.* 2002;4(5):397-401.
99. Komaba S, Takei C, Nakayama T, Ogata A, Yabuuchi N. Electrochemical intercalation activity of layered NaCrO₂ vs. LiCrO₂. *Electrochem Commun.* 2010;12(3):355-358.
100. Lu Z, Dahn JR. In Situ and ex situ XRD investigation of Li[Cr_xLi_{1/3-x/3}Mn_{2/3-2x/3}]O₂ (x = 1/3) cathode material. *J Electrochem Soc.* 2003;150(8):A1044-A1051.
101. Zhou YN, Ding JJ, Nam KW, et al. Phase transition behavior of NaCrO₂ during sodium extraction studied by synchrotron-based X-ray diffraction and absorption spectroscopy. *J Mater Chem A.* 2013;1(37):11130.
102. Masashige and Onoda. Geometrically frustrated triangular lattice system Na_xVO₂: superparamagnetism in x = 1 and trimerization in x ≈ 0.7. *J Phys Condens Matter.* 2008;20(14):145205.
103. McQueen TM, Stephens PW, Huang Q, Klimczuk T, Ronning F, Cava RJ. Successive orbital ordering transitions in NaVO₂. *Phys Rev Lett.* 2008;101(16):166402.
104. Didier C, Guignard M, Suchomel MR, Carlier D, Darriet J, Delmas C. Thermally and electrochemically driven topotactical transformations in sodium layered oxides Na_xVO₂. *Chem Mater.* 2016;28(5):1462-1471.
105. Hamani D, Ati M, Tarascon JM, Rozier P. Na_xVO₂ as possible electrode for Na-ion batteries. *Electrochem Commun.* 2011; 13(9):938-941.
106. Guignard M, Didier C, Darriet J, Bordet P, Elkaim E, Delmas C. P2-Na_xVO₂ system as electrodes for batteries and electron-correlated materials. *Nat Mater.* 2013;12(1):74-80.
107. Lu Z, Dahn J. In situ X-ray diffraction study of P2-Na_{2/3}[Ni_{1/3}Mn_{2/3}]O₂. *J Electrochem Soc.* 2001;148(11):A1225-A1229.
108. Fielden R, Obrovac MN. Investigation of the NaNi_xMn_{1-x}O₂ (0 ≤ x ≤ 1) system for Na-ion battery cathode materials. *J Electrochem Soc.* 2015;162(3):A453-A459.
109. Liu Y, Shen Q, Zhao X, et al. Hierarchical engineering of porous P2-Na_{2/3}Ni_{1/3}Mn_{2/3}O₂ nanofibers assembled by nanoparticles enables superior sodium-ion storage cathodes. *Adv Funct Mater.* 2019;30(6):1907837.
110. Wang X, Tamaru M, Okubo M, Yamada A. Electrode properties of P2-Na_{2/3}Mn_yCo_{1-y}O₂ as cathode materials for sodium-ion batteries. *J Phys Chem C.* 2013;117(30):15545-15551.
111. Bucher N, Hartung S, Franklin JB, et al. P2-Na_xCo_yMn_{1-y}O₂ (y = 0, 0.1) as cathode materials in sodium-ion batteries—effects of doping and morphology to enhance cycling stability. *Chem Mater.* 2016;28(7):2041-2051.
112. Zhu YE, Qi X, Chen X, et al. A P2-Na_{0.67}Co_{0.5}Mn_{0.5}O₂ cathode material with excellent rate capability and cycling stability for sodium ion batteries. *J Mater Chem A.* 2016;4(28): 11103-11109.
113. Shen Y, Birgisson S, Iversen BB. A P2-Na_xCo_{0.7}Mn_{0.3}O₂ (x ≈ 1.0) cathode material for Na-ion batteries with superior rate and cycle capability. *J Mater Chem A.* 2016;4(31): 12281-12288.
114. Yabuuchi N, Kajiyama M, Iwatate J, et al. P2-type Na_x[Fe_{1/2}Mn_{1/2}]O₂ made from earth-abundant elements for rechargeable Na batteries. *Nat Mater.* 2012;11(6):512-517.
115. Kalluri S, Seng KH, Wei KP, Guo Z, Dou SJAAMI. Electrospun P2-type Na_{2/3}(Fe_{1/2}Mn_{1/2})O₂ hierarchical nanofibers as cathode material for sodium-ion batteries. *ACS Appl Mater Interfaces.* 2014;6(12):8953-8958.
116. Dose WM, Sharma N, Pramudita JC, et al. Crystallographic evolution of P2 Na_{2/3}Fe_{0.4}Mn_{0.6}O₂ electrodes during electrochemical cycling. *Chem Mater.* 2016;28(17): 6342-6354.
117. Li Y, Yang Z, Xu S, et al. Air-stable copper-based P2-Na_{7/9}Cu_{2/9}Fe_{1/9}Mn_{2/3}O₂ as a new positive electrode material for sodium-ion batteries. *Adv Sci.* 2015;2(6):1500031.
118. Han MH, Gonzalo E, Sharma N, López del Amo JM, Armand M, Avdeev M. High-performance P2-phase Na_{2/3}Mn_{0.8}Fe_{0.1}Ti_{0.1}O₂ cathode material for ambient-temperature sodium-ion batteries. *Chem Mater.* 2015; 28(1):106-116.

119. Tang K, Wang Y, Zhang X, et al. High-performance P2-type Fe/Mn-based oxide cathode materials for sodium-ion batteries. *Electrochim Acta*. 2019;312:45-53.
120. Cao MH, Wang Y, Shadiké Z, et al. Suppressing the chromium disproportionation reaction in O3-type layered cathode materials for high capacity sodium-ion batteries. *J Mater Chem A*. 2017;5(11):5442-5448.
121. Zhou D, Huang W, Lv X, Zhao F. A novel P2/O3 biphasic $\text{Na}_{0.67}\text{Fe}_{0.425}\text{Mn}_{0.425}\text{Mg}_{0.15}\text{O}_2$ as cathode for high-performance sodium-ion batteries. *J Power Sources*. 2019;421:147-155.
122. de la Llave E, Talaie E, Levi E, et al. Improving energy density and structural stability of manganese oxide cathodes for Na-ion batteries by structural lithium substitution. *Chem Mater*. 2016;28(24):9064-9076.
123. Du K, Zhu J, Hu G, Gao H, Li Y, Goodenough JB. Exploring reversible oxidation of oxygen in a manganese oxide. *Energy Environ Sci*. 2016;9(8):2575-2577.
124. Kim D, Cho M, Cho K. Rational design of $\text{Na}(\text{Li}_{1/3}\text{Mn}_{2/3})\text{O}_2$ operated by anionic redox reactions for advanced sodium-ion batteries. *Adv Mater*. 2017;29(33):1701788.
125. Yang L, Li X, Ma X, et al. Design of high-performance cathode materials with single-phase pathway for sodium ion batteries: a study on P2- $\text{Na}_x(\text{Li}_y\text{Mn}_{1-y})\text{O}_2$ compounds. *J Power Sources*. 2018;381:171-180.
126. Yang L, Amo JML, Shadiké Z, et al. A Co- and Ni-free P2/O3 biphasic lithium stabilized layered oxide for sodium-ion batteries and its cycling behavior. *Adv Funct Mater*. 2020;30(42):2003364.
127. Cao X, Li H, Qiao Y, et al. Stabilizing reversible oxygen redox chemistry in layered oxides for sodium-ion batteries. *Adv Energy Mater*. 2020;10(15):1903785.
128. Yabuuchi N, Hara R, Kubota K, Paulsen J, Kumakura S, Komaba S. A new electrode material for rechargeable sodium batteries: P2-type $\text{Na}_{2/3}[\text{Mg}_{0.28}\text{Mn}_{0.72}]\text{O}_2$ with anomalously high reversible capacity. *J Mater Chem A*. 2014;2(40):16851-16855.
129. Billaud J, Singh G, Armstrong AR, et al. $\text{Na}_{0.67}\text{Mn}_{1-x}\text{Mg}_x\text{O}_2$ ($0 \leq x \leq 0.2$): a high capacity cathode for sodium-ion batteries. *Energy Environ Sci*. 2014;7(4):1387-1391.
130. Soundharrajan V, Sambandam B, Alfuruqi MH, et al. $\text{Na}_{2.3}\text{Cu}_{1.1}\text{Mn}_2\text{O}_{7-8}$ nanoflakes as enhanced cathode materials for high-energy sodium-ion batteries achieved by a rapid pyrosynthesis approach. *J Mater Chem A*. 2020;8(2):770-778.
131. Bai X, Sathiyá M, Mendoza-Sánchez B, et al. Anionic redox activity in a newly Zn-doped sodium layered oxide P2- $\text{Na}_{2/3}\text{Mn}_{1-y}\text{Zn}_y\text{O}_2$ ($0 < y < 0.23$). *Adv Energy Mater*. 2018;8(32):1802379.
132. Pang WL, Zhang XH, Guo JZ, et al. P2-type $\text{Na}_{2/3}\text{Mn}_{1-x}\text{Al}_x\text{O}_2$ cathode material for sodium-ion batteries: Al-doped enhanced electrochemical properties and studies on the electrode kinetics. *J Power Sources*. 2017;356:80-88.
133. Bhangé DS, Ali G, Kim DH, et al. Honeycomb-layer structured $\text{Na}_3\text{Ni}_2\text{BiO}_6$ as a high voltage and long life cathode material for sodium-ion batteries. *J Mater Chem A*. 2017;5(3):1300-1310.
134. Yuan D, Liang X, Wu L, et al. A honeycomb-layered $\text{Na}_3\text{Ni}_2\text{SbO}_6$: a high-rate and cycle-stable cathode for sodium-ion batteries. *Adv Mater*. 2014;26(36):6301-6306.
135. Ma J, Bo SH, Wu L, Zhu Y, Grey CP, Khalifah PG. Ordered and disordered polymorphs of $\text{Na}(\text{Ni}_{2/3}\text{Sb}_{1/3})\text{O}_2$: honeycomb-ordered cathodes for Na-ion batteries. *Chem Mater*. 2015;27(7):2387-2399.
136. Li Q, Xu S, Guo S, et al. A superlattice-stabilized layered oxide cathode for sodium on batteries. *Adv Mater*. 2020;32(23):1907936.
137. Yu H, Guo S, Zhu Y, Ishida M, Zhou H. Novel titanium-based O3-type $\text{NaTi}_{0.5}\text{Ni}_{0.5}\text{O}_2$ as a cathode material for sodium ion batteries. *Chem Commun*. 2014;50(4):457-459.
138. Maletti S, Sarapulova A, Schokel A, Mikhailova D. Operando studies on the $\text{NaNi}_{0.5}\text{Ti}_{0.5}\text{O}_2$ cathode for Na-ion batteries: elucidating titanium as a structure stabilizer. *ACS Appl Mater Interfaces*. 2019;11(37):33923-33930.
139. Vassilaras P, Kwon DH, Dacek ST, et al. Electrochemical properties and structural evolution of O3-type layered sodium mixed transition metal oxides with trivalent nickel. *J Mater Chem A*. 2017;5(9):4596-4606.
140. Chen T, Liu W, Gao H, et al. A P2-type $\text{Na}_{0.44}\text{Mn}_{0.6}\text{Ni}_{0.3}\text{Cu}_{0.1}\text{O}_2$ cathode material with high energy density for sodium-ion batteries. *J Mater Chem A*. 2018;6(26):12582-12588.
141. Wang PF, You Y, Yin YX, et al. Suppressing the P2-O2 phase transition of $\text{Na}_{0.67}\text{Mn}_{0.67}\text{Ni}_{0.33}\text{O}_2$ by magnesium substitution for improved sodium-ion batteries. *Angew Chem Int Ed*. 2016;55(26):7445-7449.
142. Tapia-Ruiz N, Dose WM, Sharma N, et al. High voltage structural evolution and enhanced Na-ion diffusion in P2- $\text{Na}_{2/3}\text{Ni}_{1/3-x}\text{Mg}_x\text{Mn}_{2/3}\text{O}_2$ ($0 \leq x \leq 0.2$) cathodes from diffraction, electrochemical and ab initio studies. *Energy Environ Sci*. 2018;11(6):1470-1479.
143. Wang PF, Yao HR, Liu XY, et al. Ti-substituted $\text{NaNi}_{0.5}\text{Mn}_{0.5-x}\text{Ti}_x\text{O}_2$ cathodes with reversible O3-P3 phase transition for high-performance sodium-ion batteries. *Adv Mater*. 2017;29(19):1700210.
144. Ramasamy HV, Kaliyappan K, Thangavel R, et al. Efficient method of designing stable layered cathode material for sodium ion batteries using aluminum doping. *J Phys Chem Lett*. 2017;8(20):5021-5030.
145. Wu X, Guo J, Wang D, Zhong G, McDonald MJ, Yang Y. P2-type $\text{Na}_{0.66}\text{Ni}_{0.33-x}\text{Zn}_x\text{Mn}_{0.67}\text{O}_2$ as new high-voltage cathode materials for sodium-ion batteries. *J Power Sources*. 2015;281:18-26.
146. Zhang XH, Pang WL, Wan F, et al. P2- $\text{Na}_{2/3}\text{Ni}_{1/3}\text{Mn}_{5/9}\text{Al}_{1/9}\text{O}_2$ microparticles as superior cathode material for sodium-ion batteries: enhanced properties and mechanism via graphene connection. *ACS Appl Mater Interfaces*. 2016;8(32):20650-20659.
147. Wang Y, Zhao F, Qian Y, Ji H. High-performance P2- $\text{Na}_{0.70}\text{Mn}_{0.80}\text{Co}_{0.15}\text{Zr}_{0.05}\text{O}_2$ cathode for sodium-ion batteries. *ACS Appl Mater Interfaces*. 2018;10(49):42380-42386.
148. Kim D, Kang SH, Slater M, et al. Enabling sodium batteries using lithium-substituted sodium layered transition metal oxide cathodes. *Adv Energy Mater*. 2011;1(3):333-336.
149. Sathiyá M, Hemalatha K, Ramesha K, Tarascon JM, Prakash AS. Synthesis, structure, and electrochemical properties of the layered sodium insertion cathode material: $\text{NaNi}_{1/3}\text{Mn}_{1/3}\text{Co}_{1/3}\text{O}_2$. *Chem Mater*. 2012;24(10):1846-1853.
150. Su J, Pei Y, Yang Z, Wang X. First-principles investigation on crystal, electronic structures and diffusion barriers of $\text{NaNi}_{1/3}\text{Co}_{1/3}\text{Mn}_{1/3}\text{O}_2$ for advanced rechargeable Na-ion batteries. *Comp Mater Sci*. 2015;98(15):304-310.
151. Li ZY, Zhang J, Gao R, Zhang H, Hu Z, Liu X. Unveiling the role of Co in improving the high-rate capability and cycling

- performance of layered $\text{Na}_{0.7}\text{Mn}_{0.7}\text{Ni}_{0.3-x}\text{Co}_x\text{O}_2$ cathode materials for sodium-ion batteries. *ACS Appl Mater Interfaces*. 2016;8(24):15439-15448.
152. Zheng L, Li J, Obrovac MN. Crystal structures and electrochemical performance of air-stable $\text{Na}_{2/3}\text{Ni}_{1/3-x}\text{Cu}_x\text{Mn}_{2/3}\text{O}_2$ in sodium cells. *Chem Mater*. 2017;29(4):1623-1631.
153. Wang PF, Guo YJ, Duan H, et al. Honeycomb-ordered $\text{Na}_3\text{Ni}_{1.5}\text{M}_{0.5}\text{BiO}_6$ ($M = \text{Ni}, \text{Cu}, \text{Mg}, \text{Zn}$) as high-voltage layered cathodes for sodium-ion batteries. *ACS Energy Lett*. 2017;2(12):2715-2722.
154. Wang QC, Meng JK, Yue XY, et al. Tuning P2-structured cathode material by Na-site Mg substitution for Na-ion batteries. *J Am Chem Soc*. 2019;141(2):840-848.
155. Wang PF, Xiao Y, Piao N, et al. Both cationic and anionic redox chemistry in a P2-type sodium layered oxide. *Nano Energy*. 2020;69:104474.
156. Cao X, Li X, Qiao Y, et al. Restraining oxygen loss and suppressing structural distortion in a newly Ti-substituted layered oxide $\text{P2-Na}_{0.66}\text{Li}_{0.22}\text{Ti}_{0.15}\text{Mn}_{0.63}\text{O}_2$. *ACS Energy Lett*. 2019;4(10):2409-2417.
157. Kaliyappan K, Li G, Yang L, Bai Z, Chen Z. An ion conductive polyimide encapsulation: new insight and significant performance enhancement of sodium based P2 layered cathodes. *Energy Stor Mater*. 2019;22:168-178.
158. Xia J, Wu W, Fang K, Wu X. Enhancing the interfacial stability of P2-type cathodes by polydopamine-derived carbon coating for achieving performance improvement. *Carbon*. 2020;157:693-702.
159. Tang K, Huang Y, Xie X, et al. The effects of dual modification on structure and performance of P2-type layered oxide cathode for sodium-ion batteries. *Chem Eng J*. 2020;384:123234.
160. Hwang JY, Oh SM, Myung ST, Chung KY, Belharouk I, Sun YK. Radially aligned hierarchical columnar structure as a cathode material for high energy density sodium-ion batteries. *Nat Commun*. 2015;6:6865.
161. Hwang JY, Myung ST, Yoon CS, Kim SS, Aurbach D, Sun YK. Novel cathode materials for Na-ion batteries composed of spoke-like nanorods of $\text{Na}[\text{Ni}_{0.61}\text{Co}_{0.12}\text{Mn}_{0.27}]\text{O}_2$ assembled in spherical secondary particles. *Adv Funct Mater*. 2016;26(44):8083-8093.
162. Li X, Wu D, Zhou YN, Liu L, Yang XQ, Ceder G. O3-type $\text{Na}(\text{Mn}_{0.25}\text{Fe}_{0.25}\text{Co}_{0.25}\text{Ni}_{0.25})\text{O}_2$: a quaternary layered cathode compound for rechargeable Na ion batteries. *Electrochem Commun*. 2014;49:51-54.
163. Cao MH, Shadik Z, Bak SM, et al. Sodium storage property and mechanism of $\text{NaCr}_{1/4}\text{Fe}_{1/4}\text{Ni}_{1/4}\text{Ti}_{1/4}\text{O}_2$ cathode at various cut-off voltages. *Energy Stor Mater*. 2020;24:417-425.
164. Wen Y, Fan J, Shi C, et al. Probing into the working mechanism of Mg versus Co in enhancing the electrochemical performance of P2-Type layered composite for sodium-ion batteries. *Nano Energy*. 2019;60:162-170.
165. Yu TY, Hwang JY, Bae IT, Jung HG, Sun YK. High-performance Ti-doped O3-type $\text{Na}[\text{Ti}_x(\text{Ni}_{0.6}\text{Co}_{0.2}\text{Mn}_{0.2})_{1-x}]\text{O}_2$ cathodes for practical sodium-ion batteries. *J Power Sources*. 2019;422(15):1-8.
166. Zhang B, Wang L, Chen X, Lu Y, Xu B, Yang W. Li and Ti Codoping to stabilize slabs of high-voltage P2-type $\text{Na}_{0.56}[\text{Li}_{0.041}\text{Mn}_{0.642}\text{Ni}_{0.221}\text{Ti}_{0.095}]\text{O}_2$. *J Alloys Compd*. 2020;824:153938.
167. Mu L, Hou Q, Yang Z, et al. Water-processable $\text{P2-Na}_{0.67}\text{Ni}_{0.22}\text{Cu}_{0.11}\text{Mn}_{0.56}\text{Ti}_{0.11}\text{O}_2$ cathode material for sodium ion batteries. *J Electrochem Soc*. 2019;166(2):A251-A257.
168. Chen T, Liu W, Liu F, et al. Benefits of copper and magnesium cosubstitution in $\text{Na}_{0.5}\text{Mn}_{0.6}\text{Ni}_{0.4}\text{O}_2$ as a superior cathode for sodium ion batteries. *ACS Appl Energy Mater*. 2018;2(1):844-851.
169. Guo S, Liu P, Yu H, Zhu Y, Chen MJAC. A layered P2- and O3-type composite as a high-energy cathode for rechargeable sodium-ion batteries. *Angew Chem Int Ed*. 2015;54(20):5894-5899.
170. Xiao J, Zhang F, Tang K, et al. Rational design of a P2-type spherical layered oxide cathode for high-performance sodium-ion batteries. *ACS Cent Sci*. 2019;5(12):1937-1945.
171. Zhao C, Ding F, Lu Y, Chen L, Hu YS. High-entropy layered oxide cathodes for sodium-ion batteries. *Angew Chem Int Ed*. 2020;59(1):264-269.
172. Zhao S, Gu H, Chen B, et al. Single-phase P2-type layered oxide with Cu-substitution for sodium ion batteries. *J Energy Chem*. 2020;43:148-154.
173. Chen T, Liu W, Zhuo Y, et al. Copper surface doping to improve the structure and surface properties of manganese-rich cathode materials for sodium ion batteries. *Mater Chem Front*. 2019;3(11):2374-2379.
174. Chen T, Liu W, Zhuo Y, et al. Na^+ /vacancies promise excellent electrochemical properties for sodium ion batteries. *Chem Eng J*. 2020;383(1):123087.
175. Deng J, Luo WB, Lu X, et al. High energy density sodium-ion battery with industrially feasible and air-stable O3-type layered oxide cathode. *Adv Energy Mater*. 2018;8(5):1701610.
176. Yuan D, He W, Pei F, et al. Synthesis and electrochemical behaviors of layered $\text{Na}_{0.67}[\text{Mn}_{0.65}\text{Co}_{0.2}\text{Ni}_{0.15}]\text{O}_2$ microflakes as a stable cathode material for sodium-ion batteries. *J Mater Chem A*. 2013;1(12):3895-3899.
177. Anang DA, Park JH, Bhang DS, et al. O3-type layer-structured $\text{Na}_{0.8}[\text{Ni}_{1/5}\text{Fe}_{1/5}\text{Co}_{1/5}\text{Mn}_{1/5}\text{Ti}_{1/5}]\text{O}_2$ as long life and high power cathode material for sodium-ion batteries. *Ceram Int*. 2019;45(17):23164-23171.
178. Rahman MM, Mao J, Kan WH, et al. An ordered P2/P3 composite layered oxide cathode with long cycle life in sodium-ion batteries. *ACS Mater Lett*. 2019;1(5):573-581.
179. Keller M, Buchholz D, Passerini S. Layered Na-ion cathodes with outstanding performance resulting from the synergetic effect of mixed P- and O-type phases. *Adv Energy Mater*. 2017;7(18):1770098.
180. Luo C, Langrock A, Fan X, Liang Y, Wang C. P2-type transition metal oxides for high performance Na-ion battery cathodes. *J Mater Chem A*. 2017;5(34):18214-18220.
181. Caballero A, Hernán L, Morales J, Sánchez L, Santos Peña J, Aranda MAG. Synthesis and characterization of high-temperature hexagonal $\text{P2-Na}_{0.6}\text{MnO}_2$ and its electrochemical behaviour as cathode in sodium cells. *J Mater Chem*. 2002;12(4):1142-1147.
182. Fang Y, Yu XY, Lou XWJAC. A practical high-energy cathode for sodium-ion batteries based on uniform P2- $\text{Na}_{0.7}\text{CoO}_2$ microspheres. *Adv Mater*. 2017;56(21):5801-5805.
183. Ma C, Alvarado J, Xu J, et al. Exploring oxygen activity in the high energy P2-type $\text{Na}_{0.78}\text{Ni}_{0.23}\text{Mn}_{0.69}\text{O}_2$ cathode material for Na-ion batteries. *J Am Chem Soc*. 2017;139(13):4835-4845.

184. Wang PF, You Y, Yin YX, Guo YG. An O3-type $\text{Na}_{0.5}\text{Mn}_{0.5}\text{O}_2$ cathode for sodium-ion batteries with improved rate performance and cycling stability. *J Mater Chem A*. 2016; 4(45):17660-17664.
185. Guo S, Yu H, Liu P, et al. High-performance symmetric sodium-ion batteries using a new, bipolar O3-type material, $\text{Na}_{0.8}\text{Ni}_{0.4}\text{Ti}_{0.6}\text{O}_2$. *Energy Environ Sci*. 2015;8(4):1237-1244.
186. Yabuuchi N, Hara R, Kajiyama M, et al. New O2/P2-type Li-excess layered manganese oxides as promising multi-functional electrode materials for rechargeable Li/Na batteries. *Adv Energy Mater*. 2014;4(13):1301453.
187. Gonzalo E, Han MH, López del Amo JM, Acebedo B, Casas-Cabanas M, Rojo T. Synthesis and characterization of pure P2- and O3- $\text{Na}_{2/3}\text{Fe}_{2/3}\text{Mn}_{1/3}\text{O}_2$ as cathode materials for Na ion batteries. *J Mater Chem A*. 2014;2(43):18523-18530.
188. Yoshida H, Yabuuchi N, Komaba S. $\text{NaFe}_{0.5}\text{Co}_{0.5}\text{O}_2$ as high energy and power positive electrode for Na-ion batteries. *Electrochem Commun*. 2013;34:60-63.
189. Guo S, Yu H, Liu D, et al. A novel tunnel $\text{Na}_{0.61}\text{Ti}_{0.48}\text{Mn}_{0.52}\text{O}_2$ cathode material for sodium-ion batteries. *Chem Commun*. 2014;50(59):7998-8001.
190. Shi WJ, Zhang D, Meng XM, et al. Low-strain reticular sodium manganese oxide as an ultrastable cathode for sodium-ion batteries. *ACS Appl Mater Interfaces*. 2020;12(12):14174-14184.
191. Li X, Guo S, Qiu F, Wang L, Ishida M, Zhou H. $\text{Na}_2\text{Ru}_{1-x}\text{Mn}_x\text{O}_3$ as the cathode for sodium-ion batteries. *J Mater Chem A*. 2019;7(9):4395-4399.
192. Clément RJ, Billaud J, Robert Armstrong A, et al. Structurally stable Mg-doped P2- $\text{Na}_{2/3}\text{Mn}_{1-y}\text{Mg}_y\text{O}_2$ sodium-ion battery cathodes with high rate performance: insights from electrochemical, NMR and diffraction studies. *Energy Environ Sci*. 2016;9(10):3240-3251.
193. Sharma N, Han MH, Pramudita JC, Gonzalo E, Brand HEA, Rojo T. A comprehensive picture of the current rate dependence of the structural evolution of P2- $\text{Na}_{2/3}\text{Fe}_{2/3}\text{Mn}_{1/3}\text{O}_2$. *J Mater Chem A*. 2015;3(42):21023-21038.
194. Singh G, Tapia-Ruiz N, Lopez del Amo JM, et al. High voltage Mg-doped $\text{Na}_{0.67}\text{Ni}_{0.3-x}\text{Mg}_x\text{Mn}_{0.7}\text{O}_2$ ($x = 0.05, 0.1$) Na-ion cathodes with enhanced stability and rate capability. *Chem Mater*. 2016;28(14):5087-5094.
195. Li ZY, Gao R, Zhang J, Zhang X, Hu Z, Liu X. New insights into designing high-rate performance cathode materials for sodium ion batteries by enlarging the slab-spacing of the Na-ion diffusion layer. *J Mater Chem A*. 2016;4(9):3453-3461.
196. Hou H, Gan B, Gong Y, Chen N, Sun C. P2-type $\text{Na}_{0.67}\text{Ni}_{0.23}\text{Mg}_{0.1}\text{Mn}_{0.67}\text{O}_2$ as a high-performance cathode for a sodium-ion battery. *Inorg Chem*. 2016;55(17):9033-9037.
197. Yoshida J, Guerin E, Arnault M, et al. New P2- $\text{Na}_{0.70}\text{Mn}_{0.60}\text{Ni}_{0.30}\text{Co}_{0.10}\text{O}_2$ layered oxide as electrode material for Na-ion batteries. *J Electrochem Soc*. 2014;161(14):A1987-A1991.
198. Xu GL, Amine R, Xu YF, et al. Insights into the structural effects of layered cathode materials for high voltage sodium-ion batteries. *Energy Environ Sci*. 2017;10(7):1677-1693.
199. Doubaji S, Valvo M, Saadoune I, Dahbi M, Edström K. Synthesis and characterization of a new layered cathode material for sodium ion batteries. *J Power Sources*. 2014; 266(15):275-281.
200. Kaliyappan K, Liu J, Xiao B, et al. Enhanced performance of P2- $\text{Na}_{0.66}(\text{Mn}_{0.54}\text{Co}_{0.13}\text{Ni}_{0.13})\text{O}_2$ cathode for sodium-ion batteries by ultrathin metal oxide coatings via atomic layer deposition. *Adv Funct Mater*. 2017;27(37):1701870.
201. Yu TY, Hwang JY, Aurbach D, Sun YK. Microsphere $\text{Na}_{0.65}[\text{Ni}_{0.17}\text{Co}_{0.11}\text{Mn}_{0.72}]\text{O}_2$ cathode material for high-performance sodium-ion batteries. *ACS Appl Mater Interfaces*. 2017;9(51): 44534-44541.
202. Xu J, Lee DH, Clément RJ, et al. Identifying the critical role of Li substitution in P2- $\text{Na}_x[\text{Li}_y\text{Ni}_z\text{Mn}_{1-y-z}]\text{O}_2$ ($0 < x, y, z < 1$) intercalation cathode materials for high-energy Na-ion batteries. *Chem Mater*. 2014;26(2):1260-1269.
203. Lee E, Lu J, Ren Y, et al. Layered P2/O3 intergrowth cathode: toward high power Na-ion batteries. *Adv Energy Mater*. 2014; 4(17):1400458.
204. Kim D, Lee E, Slater M, Lu W, Rood S, Johnson CS. Layered $\text{Na}[\text{Ni}_{1/3}\text{Fe}_{1/3}\text{Mn}_{1/3}]\text{O}_2$ cathodes for Na-ion battery application. *Electrochem Commun*. 2012;18:66-69.
205. Yoshida H, Yabuuchi N, Kubota K, et al. P2-type $\text{Na}_{2/3}\text{Ni}_{1/3}\text{Mn}_{2/3-x}\text{Ti}_x\text{O}_2$ as a new positive electrode for higher energy Na-ion batteries. *Chem Commun*. 2014;50(28): 3677-3680.
206. Wang PF, Yao HR, Liu XY, et al. Na^+ /vacancy disordering promises high-rate Na-ion batteries. *Sci Adv*. 2018;4(3):eaar6018.
207. Wu X, Jin S, Zhang Z, et al. Unraveling the storage mechanism in organic carbonyl electrodes for sodium-ion batteries. *Adv Sci*. 2015;1(8):e1500330.
208. Guo S, Liu P, Sun Y, et al. A high-voltage and ultralong-life sodium full cell for stationary energy storage. *Angew Chem Int Ed*. 2015;54(40):11701-11705.
209. Wang D, Liu Y, Wu Z, et al. A novel Mn-based P2/tunnel/O3' tri-phase composite cathode with enhanced sodium storage properties. *Chem Commun*. 2020;56(19):2921-2924.
210. Wang H, Liao XZ, Yang Y, Yan X, He YS, Ma ZF. Large-scale synthesis of $\text{NaNi}_{1/3}\text{Fe}_{1/3}\text{Mn}_{1/3}\text{O}_2$ as high performance cathode materials for sodium ion batteries. *J Electrochem Soc*. 2016;163(3):A565-A570.
211. Xiao Y, Zhu YF, Yao HR, et al. A stable layered oxide cathode material for high-performance sodium-ion battery. *Adv Energy Mater*. 2019;9(19):1803978.
212. Wang J, Zhou Z, Li Y, et al. High-rate performance O3- $\text{NaNi}_{0.4}\text{Mn}_{0.4}\text{Cu}_{0.1}\text{Ti}_{0.1}\text{O}_2$ as a cathode for sodium ion batteries. *J Alloys Compd*. 2019;792(5):1054-1060.
213. Jin T, Wang PF, Wang QC, et al. Realizing complete solid-solution reaction in a high sodium-content P2-type cathode for high-performance sodium-ion batteries. *Angew Chem Int Ed* 2020;59(34):14511-14516.
214. Oh SM, Myung ST, Hwang JY, Scrosati B, Amine K, Sun YK. High capacity O3-type $\text{Na}[\text{Li}_{0.05}(\text{Ni}_{0.25}\text{Fe}_{0.25}\text{Mn}_{0.5})_{0.95}]\text{O}_2$ cathode for sodium ion batteries. *Chem Mater*. 2014; 26(21):6165-6171.
215. Yue JL, Zhou YN, Yu X, Bak SM, Yang XQ, Fu ZW. O3-type layered transition metal oxide $\text{Na}(\text{NiCoFeTi})_{1/4}\text{O}_2$ as a high rate and long cycle life cathode material for sodium ion batteries. *J Mater Chem A*. 2015;3(46):23261-23267.
216. You Y, Kim SO, Manthiram A. A honeycomb-layered oxide cathode for sodium-ion batteries with suppressed P3-O1 phase transition. *Adv Energy Mater*. 2017;7(5): 1601698.

217. Fang T, Guo S, Jiang K, et al. Revealing the critical role of titanium in layered manganese-based oxides toward advanced sodium-ion batteries via a combined experimental and theoretical study. *Small Methods*. 2018;3(4):1800183.

AUTHOR BIOGRAPHIES



Tao Chen received his bachelor degree and master degree from Central South University, China. He is pursuing his PhD degree in Materials Science at Peking University. His current research interest includes high-efficiency catalysts and energy storage materials.



Baixue Ouyang received her bachelor's degree at Hunan Agricultural University, China. She started pursuing her master degree at Central South University in 2019. Her current research interest focuses on sodium-ion transition metal oxide cathode materials.



Xiaowen Fan received her bachelor degree at Wuhan Institute of Technology, China. She started pursuing her master degree at Central South University in 2019. Her current research interest is on zinc ion hybrid supercapacitor.



Weili Zhou started pursuing his bachelor's degree at Central South University in 2019. He current research interest is on degradation catalysts.



Weifang Liu received her bachelor's degree in Central South University, China. She received her master's degree in Polymer Physics and Chemistry and PhD degree in Chemical Engineering Technology at Central South University. She is carrying out her postdoctoral research in Hunan University under the supervision of Prof. Shuangyin Wang. Currently, she is focusing on the synthesis and characterization of energy storage materials for transition-metal oxides.



Kaiyu Liu is a professor of Chemistry and Chemical Engineering at Central South University, Changsha, China. He graduated from the Department of Mineral processing 1988 and obtained his PhD degree in 2003 from Central South University. He joined Central South University in 1998. His primary scientific interests cover the fields of new energy storage devices and related materials, including sodium-ion batteries, zinc-ion batteries, lithium-ion batteries, and supercapacitors.

How to cite this article: Chen T, Ouyang B, Fan X, Zhou W, Liu W, Liu K. Oxide cathodes for sodium-ion batteries: designs, challenges, and perspectives. *Carbon Energy*. 2022;4:170-199. <https://doi.org/10.1002/cey2.153>